REPORT DOCUMENTATION PAGE

Form Approved
OMB No. 0704-0188

1. REPORT DATE *(DD-MM-YYYY)*	2. REPORT TYPE	3. DATES COVERED *(From - To)*
xx-12-2018	Final report	October 2015 - September 2018

4. TITLE AND SUBTITLE

Multiscale materials science: a mathematical approach to defects, effective global and local behaviors and uncertainty

5a. CONTRACT NUMBER

5b. GRANT NUMBER

N00014-15-1-2777

5c. PROGRAM ELEMENT NUMBER

6. AUTHOR(S)

Le Bris, Claude; Legoll, Frederic

5d. PROJECT NUMBER

5e. TASK NUMBER

5f. WORK UNIT NUMBER

7. PERFORMING ORGANIZATION NAME(S) AND ADDRESS(ES)

Ecole Nationale des Ponts et Chaussées
6 et 8 avenue Blaise Pascal, Cité Descartes, Champs sur Marne
77455 Marne la Vallée Cedex 2, FRANCE

8. PERFORMING ORGANIZATION REPORT NUMBER

9. SPONSORING/MONITORING AGENCY NAME(S) AND ADDRESS(ES)

Same as performing organization (see block 7).

10. SPONSOR/MONITOR'S ACRONYM(S)

11. SPONSOR/MONITOR'S REPORT NUMBER(S)

12. DISTRIBUTION/AVAILABILITY STATEMENT

Distribution A (approved for public release; distribution unlimited)

13. SUPPLEMENTARY NOTES

14. ABSTRACT

We focus on developing new mathematical and numerical methods in the context of multiscale materials. We have first addressed questions related to non-periodic modelling, considering heterogeneous materials with defects. Existence and uniqueness of appropriate corrector functions has been shown, along with quantitative results on the quality of the two-scale expansion. Second, we have considered numerical questions related to the MsFEM approach. We have first developed a guaranteed and fully computable a posteriori error estimate, which gives rise to an adaptive discretization procedure. We have also studied how the MsFEM can be adapted to advection-dominated convection-diffusion equations.

15. SUBJECT TERMS

Mathematical approaches for materials science, Coarse-graining, Non-periodic multiscale materials, Defects, Multiscale Finite Element Method (MsFEM)

16. SECURITY CLASSIFICATION OF:			17. LIMITATION OF ABSTRACT	18. NUMBER OF PAGES	19a. NAME OF RESPONSIBLE PERSON
a. REPORT	b. ABSTRACT	c. THIS PAGE			19b. TELEPHONE NUMBER *(Include area code)*
				40	

École des Ponts
ParisTech

Direction de la Recherche

Defense Technical Information Center
8725 John J Kingman Road Ste 0944
Fort Belvoir, VA22060-6218
United States of América

N/Réf. : DR/PC/19-016-8J1616

Carolina GARCIA-OLMEDO
☎+33 164 15 3646
✉carolina.garcia-olmedo@enpc.fr

Champs-sur-Marne, the 25th January 2019

SUBJECT: N00014-15-1-277 – Multiscale materials science: a mathematical approach to defects, effective global and local behaviours and uncertainty - Reports

Dear Madame, Sir,

Our project "Multiscale materials science: a mathematical approach to defects, effective global and local behaviours and uncertainty" was concluded the 29th September 2018.

As request on the Award Modification, you will find enclosed the following reports:

- Final Technical Report with SF298

Should you have any question, please do not hesitate to contact us.

Yours faithfully,

Carolina GARCIA-OLMEDO
Chargée d'affaires et développement de la recherche partenariale

Contract N00014-15-1-2777

Multiscale materials science: a mathematical approach to defects, effective global and local behaviors and uncertainty

Report to the Office of Naval Research

C. Le Bris and F. Legoll

October 2015 – September 2018

Contents

1 Introduction **2**

2 Modeling of defects **4**

3 A posteriori error estimation for MsFEM computations **7**
- 3.1 Model problem 8
- 3.2 Overview of MsFEM 9
  - 3.2.1 Linear-MsFEM approximation 10
  - 3.2.2 Nonconforming MsFEM approximation: the oversampling technique . . 10
- 3.3 *A posteriori* error estimation using CRE and adaptive strategy 12
  - 3.3.1 Basics on CRE 12
  - 3.3.2 Construction of an equilibrated flux field 13
  - 3.3.3 Adaptive discretization 15
- 3.4 Numerical results 16

4 MsFEM approaches for advection dominated problems in perforated domains **19**
- 4.1 Presentation of our numerical approaches 21
  - 4.1.1 MsFEM approaches using only the diffusion operator, and their stabilized version 22
  - 4.1.2 MsFEM approaches using the full advection-diffusion operator, and their stabilized version 24
- 4.2 Homogenization results 25
- 4.3 Numerical results 27
  - 4.3.1 A periodic case 28
  - 4.3.2 A non-periodic case 35

5 Conclusion and perspectives **35**

References **38**

1 Introduction

We report here on the work performed during the three years (October 1st, 2015 - September 30th, 2018) of the contract N00014-15-1-2777 on *Multiscale materials science: a mathematical approach to defects, effective global and local behaviors and uncertainty.*

The presence of numerous length-scales in material science problems represents a daunting challenge for numerical simulation. The bottom line of our long-term project is to develop new mathematical and numerical tools, including probabilistic approaches, to address the current challenging problems of interest in materials science. In particular, one major feature of the project is to address questions using both deterministic approaches and probabilistic approaches. It is our belief that a satisfactory theoretical understanding of ideal *perfect* materials has now been achieved along with the design of reasonably efficient numerical approaches for the simulation of those. It is however a pending challenge to understand, model, simulate and control *real* materials in all their inevitable imperfections. Issues such as the modeling of defects, of how fatigue and aging affect the characteristic of materials, are not so well understood. Clearly, research in this matter requires skills diverse in nature. The present project in particular aims at suggesting mathematical approaches that can help in this endeavor.

The first track that we mentioned in our original proposal was concerned with the development of methods to approximate a problem with highly oscillatory coefficients by a problem with coarse coefficients. Our aim was to define and construct the best non-oscillating coefficient $\overline{A}$ (think e.g. of a constant coefficient) that is consistent, in a sense to be made precise, with the behavior of a heterogeneous material modelled by a highly oscillatory coefficient $A^\varepsilon(x)$. Such an approach can be considered as an alternative pathway to standard homogenization techniques when these latter are difficult to use in practice, in particular when information is missing on the coefficient $A^\varepsilon(x)$. Of course, modelling the material with $\overline{A}$ (rather than $A^\varepsilon(x)$) yields much more affordable approaches, since there is no fast frequency in that coefficient. A central question, intimately related to homogenization theory, is to construct in an efficient manner this best constant coefficient.

This topic has been early dealt with. We have collected our results (in particular for what concerns the approximation of the *gradient* of the highly oscillatory solution) in the article [7], and do not report any further on this topic here.

In Section 2 of this report, we address questions related to non-periodic modelling of multiscale materials, in line with the second track of our original proposal. Random modelling is indeed a standard modelling response to situations when the idealized, say periodic, modelling is inappropriate. It is however commonly admitted, and observed in practice, that random modelling leads to possibly prohibitively computationally expensive problems. There is a definite theoretical and practical interest in generalizing modelling of perfect materials in directions different from the random paradigm.

Within the current contract, we have investigated this idea by considering heterogeneous materials with defects. The approach we have undertaken, which is described in Section 2, consists in considering an elliptic equation with oscillatory coefficients, in the case when these coefficients consist of a "nice" function (say periodic) which is perturbed by a local defect modelled as a function in $L^p(\mathbb{R}^d)$. With the works now accomplished, homogenization theory for this type of equations is essentially on the same mathematical footing as periodic homogenization is. Existence and uniqueness of corrector functions with appropriate integrability

properties have been established, in particular thanks to new Calderòn-Zygmund type estimates. Based on this, quantitative results on how the two-scale expansion approximates the exact oscillatory solution have been obtained.

In the sequel of this report, we turn to numerical approaches. Many partial differential equations of materials science involve highly oscillatory coefficients and thus small length-scales. When the microstructure of the materials is periodic, or random and statistically homogeneous, or "periodic + defect", homogenization theory can be used, and allows to appropriately define averaged equations from the original oscillatory equations. When no such structural assumption (e.g. periodicity) on the materials microstructure can be made, homogenization theory still holds, but does not provide any explicit formulae amenable (even possibly after some approximation) to numerical computations. One possibility is then to directly address the original problem (rather than passing to the limit of infinite scale separation), and to use dedicated numerical approaches for such multiscale problems, such as the Multiscale Finite Element Method (MsFEM). Recall that the MsFEM method consists of

- an "offline" stage, where highly oscillatory basis functions are numerically computed as solutions to local problems (that mimick in a suitable way the reference problem on a subdomain). These basis functions are thus expected to be well-adapted to the problem at hand.

- an "online" stage, where a Galerkin approximation of the reference problem is solved. The approximation is performed in the finite dimensional space spanned by the basis functions computed in the prior offline stage.

In Section 3, we consider a classical multiscale diffusion problem discretized by MsFEM, and introduce quantitative and robust tools to control the numerical accuracy of the approximate solution. We build a guaranteed and fully computable *a posteriori* error estimate for the global error measured in the energy norm. This estimate is based on the Constitutive Relation Error (CRE) concept, with the computation of equilibrated fluxes as a post-treatment of the approximate MsFEM solution. This estimate can next be used to drive an adaptive procedure, where the discretization parameters are adapted in order to reach a required accuracy at the smallest computational cost.

In Section 4, we next turn to an advection-diffusion equation that is advection-dominated and posed on a perforated domain. There are two small scales in the problem. The first small scale is the size of the perforations, which is of the same order of magnitude as the distance between two neighboring perforations. The second small scale is related to the ratio between diffusion and convection. In addition to the difficulty owing to the presence of different scales, the strong convection is also a source of potential instabilities. Taken *separately*, each phenomenon can be addressed by classical approaches: MsFEM type approaches and stabilized type techniques (e.g. the Streamline Upwind Petrov-Galerkin (SUPG) method), respectively. The purpose of this work is to investigate the behavior of several variants of MsFEM type methods. We present, study and compare various options in terms of choice of basis elements, adjunction of bubble functions and stabilized formulations.

The works described below have been performed (jointly or separately) by Claude Le Bris (PI) and Frédéric Legoll (Co-PI), along with various external collaborators. Thanks to the

specific support of ONR to the research activity of our group, we have been able to hire in our group Simon Lemaire (postdoctoral fellow) and François Madiot (PhD student), who both have contributed to this research program.

2 Modeling of defects

[Work expanded in [1, 2, 3, 4]].

Modeling of heterogeneous materials with defects at the small scale is a long-term endeavor that has been consistently supported by the funding of ONR through the previous two contracts (from 2009 through 2015, see e.g. [15]) and the present contract on the period October 2015 – September 2018 (along with a similar funding support by EOARD on the same general topic over the same periods). These defects, usually microscopic, are of paramount importance for the understanding of the behavior of materials, even at the macroscopic scale.

Let us summarize the context and the achievements. Typically, consider a periodic material (where the period is small with respect to the size of the sample, so that there exists a separation of scales between the microstructure and the macrostructure, see e.g. [20] for more details), with a superimposed defect in *one* (or "a few", meaning a perturbation dying down "at infinity") periodic cells. A typical equation modeling such a situation reads as

$$-\mathrm{div}\left[\left(A_{\mathrm{per}}\left(\frac{x}{\varepsilon}\right)+B_{\mathrm{def}}\left(\frac{x}{\varepsilon}\right)\right)\nabla u_\varepsilon\right]=f \ \text{ in } \Omega, \tag{1}$$

where the perturbation B_{def} is localized (in the sense that B_{def} vanishes at infinity, a property that is later encoded as $B_{\mathrm{def}} \in L^p(\mathbb{R}^d)$ for some $p < +\infty$, even though this assumption does not cover the full generality of $B_{\mathrm{def}}(x) \overset{|x|\to+\infty}{\longrightarrow} 0$), while A_{per} encodes the perfect, periodic medium. From the macroscopic standpoint, the overall behavior might, or not, be the same as that of a perfect periodic material. Anyhow, close to the defect (i.e. close to the "support" of B_{def}), the response is of course very different from that of the perfect material.

The long term goal is, beyond the theoretical understanding, to develop numerical approaches to efficiently and accurately capture how the presence of such defects affect, either locally or globally, the behavior of the considered material.

The mathematical endeavor is conducted by Claude Le Bris, in external collaboration with Xavier Blanc (University Paris Diderot) and Pierre-Louis Lions (Collège de France), neither of these collaborators being an investigator of the present contract. Some students, both at the master level and the PhD level, and supervised or co-supervised by Claude Le Bris, may also participate. For the funding period 2015-2018, some works (see the publications [1, 2]) have been accomplished by such a PhD student, namely Marc Josien, the salary of whom was covered by another source of funding.

The previous funding periods until 2015 have seen significant progress along this line of research. They all concern *linear elliptic equations* (or *systems*, and this is a major variant because their study is orders of magnitude more difficult than those of *equations* – because in particular of the absence of maximum principles in many situations, which dramatically restricts the available techniques of proofs). The publication [9], dating back to 2012 and completed during a previous funding period, addressed the precise case of equation (1) for a

perturbation $B_{\text{def}} \in L^2(\mathbb{R}^d)$. Then the case of defects $B_{\text{def}} \in L^p(\mathbb{R}^d)$ for $1 < p < +\infty$ possibly different from 2 (which is considerably more difficult than the case $p = 2$ because there is no Hilbertian structure then) was considered in the next two publications [10, 11], mentioned in the previous contract. Existence (and uniqueness up to additive constants) of corrector functions w_p, that is, solutions for $p \in \mathbb{R}^d$ fixed to

$$-\text{div}\left[\left(A_{\text{per}} + B_{\text{def}}\right)\left(p + \nabla w_p\right)\right] = 0 \quad \text{in } \mathbb{R}^d,$$

were proven. Put differently, we have shown existence of small scale corrections to the overall averaged behavior encoded in the solution to the homogenized equation associated to (1).

In standard (say, periodic) settings, the existence of such corrector functions is enough to guarantee the existence of a precise approximation $u^\star(x) + \varepsilon \sum_{j=1}^{d} w_{e_j}(x/\varepsilon)\, \partial_{x_j} u^\star(x)$ of the oscillatory solution u_ε, where of course $u^\star$ is the solution to the homogenized equation

$$-\text{div}\left(A^\star \nabla u^\star\right) = f \quad \text{in } \Omega.$$

This was indeed conjectured and formally proven in the publications [9, 10, 11], but the exact mathematical proofs were still to be performed in the presence of defects.

This task was precisely accomplished during the present funding period, in the publications [1, 2, 3, 4]. But actually more facts were proven therein.

First, a new, more versatile proof of the result originally given in [10, 11] was introduced in [3]. Second, this versatility was exploited to extend the results to other (still linear) equations, this time not necessarily in divergence form, namely equations of the type

$$-\left[A_{\text{per}}\left(\frac{x}{\varepsilon}\right) + B_{\text{def}}\left(\frac{x}{\varepsilon}\right)\right]_{ij} \partial_{ij} u_\varepsilon = f \quad \text{in } \Omega.$$

Likewise, and this was the focus of [4], the advection-diffusion equation (a major equation for practically relevant cases)

$$-\text{div}\left[\left(A_{\text{per}}\left(\frac{x}{\varepsilon}\right) + B_{\text{def}}\left(\frac{x}{\varepsilon}\right)\right)\nabla u_\varepsilon\right] + \left[C_{\text{per}}\left(\frac{x}{\varepsilon}\right) + D_{\text{def}}\left(\frac{x}{\varepsilon}\right)\right] \cdot \nabla u_\varepsilon = f \quad \text{in } \Omega \qquad (2)$$

(with self-explanatory notation) was addressed. Central to the new proof and to several results that allow one to extend the study to these other equations are the linear *a priori estimates* of the Calderòn-Zygmund type:

$$\|\nabla v\|_{L^q(\mathbb{R}^d)} \leq C_q \, \|g\|_{L^q(\mathbb{R}^d)}$$

for general solutions v to equations (or systems) of the form

$$-\text{div}(a \nabla v) = \text{div}\, g \quad \text{in } \mathbb{R}^d$$

for vector-valued functions g, or alternately

$$\left\|D^2 v\right\|_{L^q(\mathbb{R}^d)} \leq C_q \, \|g\|_{L^q(\mathbb{R}^d)}$$

for equations of the form

$$-a_{ij}\, \partial_{ij} v = g \quad \text{in } \mathbb{R}^d$$

for scalar-valued functions g. Most of the work accomplished consists in generalizing these estimates from the case a constant (the actual Calderòn-Zygmund estimates) to the case a periodic (which has been completed by M. Avellaneda and F.H. Lin in their seminal series of articles of the late 1980s [17, 18, 19]), and next to the case a "periodic + defect", which we achieved. Given that we deal here with *linear* equations (or, again, systems), it is intuitive (and this turns out to be a mathematical reality) that these estimates allow to conclude to the right existence and uniqueness theorems.

As for the more difficult advection-diffusion equation (2), the strategy consists in establishing the existence of the suitable invariant measure associated to the equation, a fact which is in turn established by duality, based upon some of the above results. One next uses the invariant measure to transform equation (2) into a divergence form equation of the type (1). And one concludes using the general results just proven for such an equation.

In addition to this, we pursued one of the directions announced in our proposal for the present funding period. In 2015, we announced that we were interested in the case when a *singular right-hand side* is inserted in equation (1). We had precisely in mind to consider right-hand sides $f \notin H^{-1}$ in (1). We readily realized that the question under examination was very much related to the question of the determination of the Green function for the differential operator of the left-hand side of (1). Indeed, a typical $f \notin H^{-1}$ is f the Dirac mass, in which case the solution u_ε is exactly the Green function G_ε. In turn, understanding the behavior of the Green function G_ε is key to indeed prove quantitative estimates for the approximation of u_ε, as shown in the series of works [17, 18, 19] already cited above. Therefore, the two questions of (i) using the corrector we constructed in previous works for the actual approximations of the solutions and (ii) investigating the behavior of the solution for singular right-hand sides, are closely related, not to say almost identical.

We settled these issues in our publications [1, 2]. We now have at our disposal a complete quantitative theory, at least for the case of defects in the equation (1) that are in $L^p(\mathbb{R}^d)$, $p < +\infty$ (and likewise for the related systems, and equations mentioned above). The rate ε^ν with which $u^\star(x) + \varepsilon \sum_{j=1}^{d} w_{e_j}(x/\varepsilon)\, \partial_{x_j} u^\star(x)$ approximates u_ε in suitable norms for ε small, or put differently, the rate with which the remainder

$$R^\epsilon(x) := u_\varepsilon(x) - u^\star(x) - \varepsilon \sum_{j=1}^{d} w_{e_j}\left(\frac{x}{\varepsilon}\right) \partial_{x_j} u^\star(x)$$

vanishes as ε vanishes, is now well documented. The exponent ν explicitly depends upon the integrability $L^r(\mathbb{R}^d)$ of the defect $B_{\text{def}}(x)$ as $|x| \longrightarrow +\infty$, and the functional norm chosen to evaluate the remainder. In particular, the L^∞ norm can be used, and the result then reads

$$\|\nabla R^\varepsilon\|_{L^\infty(\Omega_1)} \leq C\varepsilon^{\nu_r} \ln\left(2 + \varepsilon^{-1}\right) \|f\|_{C^{0,\beta}(\Omega)},$$

where $\nu_r := \min(1, d/r) \in (0, 1]$, r being the integrability of the defect, and the constant C being independent from ε and f sufficiently regular (in the above estimate, Ω_1 is any bounded open set such that $\overline{\Omega_1} \subset \Omega$). This explicitly quantifies how defects can be seen at the macro scale. In a nutshell, homogenization theory for this equation in the above setting is exactly on the same mathematical footing as periodic homogenization is. Evidently, the natural research path is now to move on to the case of equations and systems other than linear ...

On the other hand, we were unable so far to proceed in the other two directions of research originally mentioned in the 2015 proposal, namely

- the case when the defect, in contrast to the cases considered so far in the works mentioned above and previously conducted, has a full *one (or two) dimensional structure* (and is therefore *not* localized), such as an interface between two different periodic structures or a skew-dislocation, and
- the case of a discrete differential operator at the micro scale where we replace equation (1) by a similar equation where the divergence and gradient operators are *discrete*.

We hope to be able to return to some of these problems (in particular the former, which we find particularly interesting and practically relevant) in the future.

3 A posteriori error estimation for MsFEM computations

[Work expanded in [5, 6]].

Developing multiscale numerical methods for problems with highly heterogeneous material structure is a very active research field. In the last twenty years, a lot of efforts have been put in the design of multiscale approaches for elliptic PDEs. They are inspired by the framework of the Finite Element Method (FEM) but take into account scale separation between macroscopic and microscopic features. Many methods have been proposed in that direction, sharing the idea of adapting the approximation space to the particular fine-scale features of the problem. We focus here on the Multiscale Finite Element Method (MsFEM), where basis functions are obtained from fine-scale, localized problems [21].

The MsFEM defines an approximate solution in a finite dimensional space, related to a macroscopic mesh and generated by basis functions that encode details of the fine-scale heterogeneities. As said in the above introduction, MsFEM performs the computations in a two-stage procedure: (i) an *offline* stage in which basis functions are computed as the solutions to local fine-scale problems; (ii) an *online* stage in which an inexpensive Galerkin approximation problem is solved. We refer to Section 3.2 below for more details. As for any numerical method, a crucial issue is to control the accuracy of the obtained approximation, and to design algorithms yielding discretizations that comply with a prescribed tolerance on the error.

Many tools have been developed for the estimation of the discretization error and the adaptation of discretization parameters in the (single scale) framework of FEM (see e.g. [25] for a review). In contrast to *a priori* estimates that establish a convergence order (with respect to discretization parameters) of a given numerical method, *a posteriori* error estimates provide quantitative information on the error as well as criteria for mesh adaptation. Various *a posteriori* error estimation tools have been introduced, many of them requiring the computation (by post-processing the approximate solution) of flux fields that satisfy equilibrium in a strong sense [25]. This enables to derive, in a convenient way, fully computable (i.e. without

any unknown multiplicative constant) and guaranteed error bounds on both the global solution (error in energy norm) and given quantities of interest (goal-oriented error estimation) using an adjoint problem.

In the multiscale framework, and for MsFEM-like methods particularly, very few *a posteriori* error estimation tools are available. One work we wish to cite is the approach [23] using the explicit residuals method. This approach, splitting the error estimate with respect to the different error sources, is effective to drive an adaptive algorithm. However, it does not enable to quantify the error level accurately (but only up to some unknown constants), which may be a drawback when certification of the accuracy and stopping criteria for adaptive algorithms are required.

In [5], we have developed a robust *a posteriori* error estimate, as well as an associated adaptive strategy, for MsFEM computations. Our approach is based on the Constitutive Relation Error (CRE) idea, a popular concept in (single scale) FEM approaches, that we have extended to the multiscale framework. We also refer to [6] for the extension of this work to goal-oriented error estimation problems.

The model problem we have considered is described in Section 3.1. Basics on MsFEM are recalled in Section 3.2. The reader familiar with the approach can skip this section and directly proceed to Section 3.3 to discover our main contributions on the topic. The *a posteriori* error estimation method based on CRE is introduced in Section 3.3 (the adaptive strategy, associated to indicators related to various error sources, is briefly mentioned in Section 3.3.3). We show there how equilibrated fluxes can be recovered from an extension of the method given for FEM in [25], so that a guaranteed and fully computable error estimate on the overall error can be derived. Some numerical experiments illustrating the performances of the proposed approach are discussed in Section 3.4. We refer to [5] for other numerical results. All these results confirm the practical interest of the proposed technique, in terms of both certification of the numerical solution and adaptive discretizations.

3.1 Model problem

We consider the highly oscillatory problem

$$-\mathrm{div}(A^\varepsilon \nabla u^\varepsilon) = f \ \text{ in } \Omega, \qquad u^\varepsilon = 0 \ \text{ on } \partial\Omega, \tag{3}$$

where Ω is an open bounded domain of $\mathbb{R}^d$, and where the loading $f \in L^2(\Omega)$ is slowly varying (it does not depend on ε).

The matrix $A^\varepsilon \in (L^\infty(\Omega))^{d\times d}$ is a rapidly oscillating function, ε representing the typical (presumably small) size of the heterogeneities. We assume that A^ε is symmetric and that it is (uniformly in x and ε) bounded from above and away from 0. The weak formulation of (3) consists in finding $u^\varepsilon \in H^1_0(\Omega)$ such that

$$\forall v \in H^1_0(\Omega), \quad B^\varepsilon(u^\varepsilon, v) = F(v), \tag{4}$$

where

$$B^\varepsilon(u,v) = \int_\Omega [A^\varepsilon \nabla u] \cdot \nabla v, \qquad F(v) = \int_\Omega f\, v.$$

The symmetric bilinear form B^ε induces the energy norm $|||v||| = \sqrt{B^\varepsilon(v,v)}$ on $H^1_0(\Omega)$.

Let $\mathcal{T}_H$ be a partition of Ω. Introducing the P1-Lagrange finite dimensional space V_H^0, the Finite Element (FE) approximation of (3) reads:

$$\text{Find } u_H \in V_H^0 \text{ such that, for any } v \in V_H^0, \quad B^\varepsilon(u_H, v) = F(v).$$

Since A^ε varies at the scale ε, it is well known that obtaining an accurate approximation u_H requires to choose $H \ll \varepsilon$. The number of degrees of freedom is then very large. This leads to a usually prohibitive computational complexity.

3.2 Overview of MsFEM

The main idea in the MsFEM approach is to construct a set $\{\phi_i^\varepsilon\}_{1\leq i\leq I}$ of local multiscale basis functions that encode small scale information within each element of a coarse mesh $\mathcal{T}_H$ ($H \gg \varepsilon$). The basis functions ϕ_i^ε, associated with each node i of the coarse mesh $\mathcal{T}_H$, are adapted to the local properties of the operator. They are pre-computed in an *offline* stage, over each element K of the coarse mesh (see Figure 1), as solutions to local elliptic equations of the form

$$-\text{div}\big[A^\varepsilon \nabla \phi_i^\varepsilon\big] = 0 \quad \text{in } K, \tag{5}$$

complemented with various boundary conditions discussed below (see e.g. (6)). In practice, the local problems (5) are solved numerically using a fine mesh of characteristic size $h < \varepsilon$.

Note that the problems (5) are decoupled one from each other. They can hence be solved in parallel.

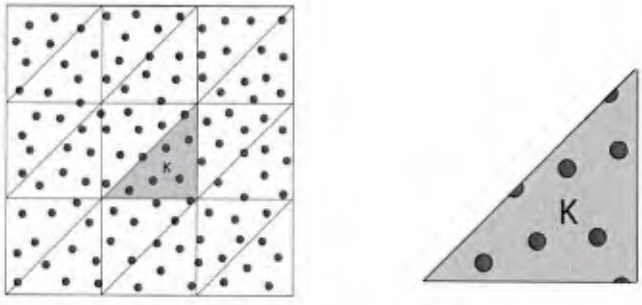

Figure 1: Left: a coarse mesh of the domain Ω is introduced, with elements of diameter H much larger than the small characteristic size ε of the heterogeneities (here the diameter of the inclusions). Right: on each coarse element, we solve a local problem, using in practice a discretization at the size h adapted to the heterogeneities.

Once the multiscale basis functions are computed, the MsFEM strategy is the same as that of a classical FE approach. It consists in performing a Galerkin approximation of (4) on

$$V_H^\varepsilon = \text{Span}\{\phi_i^\varepsilon,\ 1 \leq i \leq I\}.$$

In an *online* stage, we thus look for the approximate solution $u_H^\varepsilon \in V_H^\varepsilon$ such that

$$\forall v \in V_H^\varepsilon, \quad B^\varepsilon(u_H^\varepsilon, v) = F(v).$$

The small scale information incorporated in the basis functions is thus brought to the large scales through couplings in the global stiffness matrix. The assembly of this matrix is inexpensive since it reuses local matrices computed and stored in the *offline* stage when solving (5).

In practice, it is common to perform multiple runs for the same medium, with different boundary conditions or loadings f in (3). Since the local problems (5) are independent of these, the *offline* stage in MsFEM is done only once in such a multi-query context.

3.2.1 Linear-MsFEM approximation

The boundary conditions associated to (5) in the construction of basis functions are of critical importance, since they determine the behavior of the numerical approximation u_H^ε on the edges $\cup_{K\in\mathcal{T}_H}\partial K$ of the mesh and how this behavior may be different from that of the exact solution u^ε.

A first choice, leading to a conforming numerical discretization, is to impose a linear evolution of ϕ_i^ε along ∂K as for classical first-order FE basis functions. We thus introduce the piecewise affine FE basis functions ϕ_i^0 over the coarse mesh $\mathcal{T}_H$, $1 \leq i \leq I$, and consider the local problems

$$-\mathrm{div}\left[A^\varepsilon \nabla \phi_i^\varepsilon\right] = 0 \quad \text{in } K, \qquad \phi_i^\varepsilon = \phi_i^0 \quad \text{on } \partial K. \tag{6}$$

Note that the support of ϕ_i^ε is identical to that of ϕ_i^0. The multiscale basis functions ϕ_i^ε defined by (6) satisfy a partition of unity property, i.e. $\sum_{i=1}^{I} \phi_i^\varepsilon = 1$, a property which is useful in Section 3.3.2 below.

In the regime of interest $H \geq \varepsilon$, and assuming that the oscillations in the material behavior are *periodic*, i.e. that $A^\varepsilon(x) = A_{\mathrm{per}}(x/\varepsilon)$ for a fixed periodic matrix A_{per}, the following *a priori* error estimate holds (see [21]):

$$\|u^\varepsilon - u_H^\varepsilon\|_{H^1(\Omega)} \leq C\left(H + \sqrt{\varepsilon/H} + \sqrt{\varepsilon}\right), \tag{7}$$

where C is a positive constant independent of ε and H. The estimate (7) shows that the MsFEM approach converges to the correct solution in the homogenization limit (namely when first $\varepsilon \to 0$ and next $H \to 0$, which is the regime of interest).

3.2.2 Nonconforming MsFEM approximation: the oversampling technique

The accuracy of the Linear-MsFEM variant is limited, due to the boundary conditions imposed in (6). Indeed, in the vicinity of ∂K, u^ε oscillates (as it does everywhere in Ω), whereas the basis functions ϕ_i^ε (and thus u_H^ε) do not, as a consequence of the non-oscillatory boundary conditions $\phi_i^\varepsilon = \phi_i^0$ on ∂K. A possible remedy is to impose (incorrect) Dirichlet boundary conditions not on ∂K, but further away, on the boundary of a domain S_K which is slightly larger than K, and to only use the interior information, on K, to construct the basis functions (see Figure 2). This is the well-known oversampling technique. The approach thus consists in first solving the local problems

$$-\mathrm{div}\left[A^\varepsilon \nabla \psi_i^{\varepsilon,K}\right] = 0 \quad \text{in } S_K, \qquad \psi_i^{\varepsilon,K} \text{ is affine on } \partial S_K, \qquad \psi_i^{\varepsilon,K}(s_j) = \delta_{ij},$$

where S_K is a domain which is homothetic to the mesh element K and s_j are the coordinates of the vertices of S_K. Second, the MsFEM basis functions are defined by

$$\phi_i^\varepsilon = \psi_i^{\varepsilon,K}\Big|_K \quad \text{in } K.$$

This approach is more costly than the one presented in Section 3.2.1 since the local problems are set on larger domains.

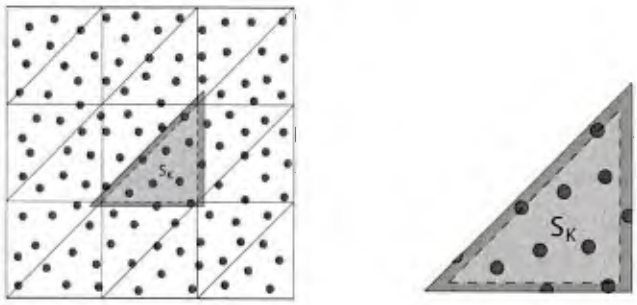

Figure 2: Illustration of the oversampling technique: a domain S_K, which is slightly larger than K, is introduced to solve the local fine scale problems.

Note that a unique basis function ϕ_i^ε is associated to each mesh node i. The basis function ϕ_i^ε may be discontinuous on the element boundaries, i.e. across ∂K. Here again, they satisfy a partition of unity property.

Once the multiscale basis functions ϕ_i^ε have been computed, a Galerkin approximation of (4) on the finite dimensional space $V_H^\varepsilon = \text{Span}\{\phi_i^\varepsilon,\ 1 \le i \le I\}$ is performed. Note however that $V_H^\varepsilon \not\subset H_0^1(\Omega)$. The global problem is then defined as

$$\text{Find } u_H^\varepsilon \in V_H^\varepsilon \text{ such that, for any } v \in V_H^\varepsilon, \quad B_H^\varepsilon(u_H^\varepsilon, v) = F(v),$$

with

$$B_H^\varepsilon(u,v) = \sum_{K\in\mathcal{T}_H} \int_K [A^\varepsilon \nabla u]\cdot\nabla v = \int_\Omega [A^\varepsilon \nabla_H u]\cdot\nabla_H v,$$

where we have set $\nabla_H u = \sum_{K\in\mathcal{T}_H} 1_K\, \nabla u|_K$ and likewise for v.

In [22], an *a priori* error estimate is derived for the oversampling variant of the MsFEM approach. In the case $H \gg \varepsilon$ and in the periodic setting, assuming that the distance between K and ∂S_K is of order H, the estimate reads

$$\left(\sum_{K\in\mathcal{T}_H} \|u^\varepsilon - u_H^\varepsilon\|^2_{H^1(K)}\right)^{1/2} \le C_1 H + C_2\frac{\varepsilon}{H} + C_3\sqrt{\varepsilon}, \tag{8}$$

where C_1, C_2 and C_3 are independent of ε and H, and C_2 depends on the oversampling ratio. Since the approach is non-conforming, the error is measured in the broken H^1-norm.

The estimate (8) is better than the one without oversampling (namely (7)), since the leading order term $\sqrt{\varepsilon/H}$ (due to boundary effects on $\cup_{K\in\mathcal{T}_H}\partial K$) is now replaced by the term ε/H. This theoretical result, as well as numerous numerical results, show that the oversampling variant outperforms the Linear-MsFEM variant.

3.3 *A posteriori* error estimation using CRE and adaptive strategy

In this section, we derive a guaranteed upper bound on the error in the energy norm $|||u^\varepsilon - u_H^\varepsilon|||$. For the sake of simplicity, we restrict ourselves to the case of conforming approximations $V_H^\varepsilon \subset H_0^1(\Omega)$, although the approach can be extended to non-conforming approximations. The method is based on the Constitutive Relation Error (CRE) concept, which has been successfully used in (single-scale) FEM simulations.

3.3.1 Basics on CRE

We introduce the space of equilibrated fluxes

$$W = \left\{ \boldsymbol{p} \in [L^2(\Omega)]^d, \quad \operatorname{div} \boldsymbol{p} \in L^2(\Omega), \quad \operatorname{div} \boldsymbol{p} + f = 0 \text{ in } \Omega \right\}.$$

Any flux field $\widehat{\boldsymbol{p}} \in W$ satisfies the following relation:

$$\forall v \in H_0^1(\Omega), \quad \int_\Omega \widehat{\boldsymbol{p}} \cdot \nabla v = \int_\Omega f\, v. \tag{9}$$

Then, for any $\widehat{u}^\varepsilon \in H_0^1(\Omega)$ and for any flux field $\widehat{\boldsymbol{p}} \in W$, we define the CRE functional E_{CRE} as

$$\left(E_{\mathrm{CRE}}\left(\widehat{u}^\varepsilon, \widehat{\boldsymbol{p}}\right)\right)^2 = \int_\Omega (A^\varepsilon)^{-1}(\widehat{\boldsymbol{p}} - A^\varepsilon \nabla \widehat{u}^\varepsilon) \cdot (\widehat{\boldsymbol{p}} - A^\varepsilon \nabla \widehat{u}^\varepsilon).$$

Since $V_H^\varepsilon \subset H_0^1(\Omega)$, we can choose $\widehat{u}^\varepsilon = u_H^\varepsilon$. It is next easy to show that

$$\forall \widehat{\boldsymbol{p}} \in W, \qquad |||u^\varepsilon - u_H^\varepsilon||| \leq E_{\mathrm{CRE}}(u_H^\varepsilon, \widehat{\boldsymbol{p}}). \tag{10}$$

Indeed, using an integration by parts and denoting $\boldsymbol{q}^\varepsilon = A^\varepsilon \nabla u^\varepsilon$, we have

$$\begin{aligned}
|||u^\varepsilon - u_H^\varepsilon|||^2 &= \int_\Omega (\boldsymbol{q}^\varepsilon - A^\varepsilon \nabla u_H^\varepsilon) \cdot \nabla (u^\varepsilon - u_H^\varepsilon) \\
&= \int_\Omega (\widehat{\boldsymbol{p}} - A^\varepsilon \nabla u_H^\varepsilon) \cdot \nabla (u^\varepsilon - u_H^\varepsilon) + \int_\Omega (f + \operatorname{div} \widehat{\boldsymbol{p}})(u^\varepsilon - u_H^\varepsilon) \\
&= \int_\Omega (\widehat{\boldsymbol{p}} - A^\varepsilon \nabla u_H^\varepsilon) \cdot \nabla (u^\varepsilon - u_H^\varepsilon) \\
&\leq E_{\mathrm{CRE}}(u_H^\varepsilon, \widehat{\boldsymbol{p}})\, |||u^\varepsilon - u_H^\varepsilon|||.
\end{aligned}$$

The bound (10) implies that a guaranteed upper bound on the error $|||u^\varepsilon - u_H^\varepsilon|||$ is obtained from any flux field $\widehat{\boldsymbol{p}} \in W$. Its quality is ensured by a suitable choice of $\widehat{\boldsymbol{p}}$.

Remark 1 *The CRE concept has also been used to establish error bounds on quantities of interest (goal-oriented error estimation) using an adjoint problem. We refer to [6] for the extension of this approach to MsFEM computations.*

3.3.2 Construction of an equilibrated flux field

The technical point in the CRE concept is the construction of a relevant admissible flux $\widehat{\boldsymbol{p}} \in W$. Several methods can be used. We use here a method referred as the Hybrid-Flux Technique, or Element Equilibration Technique (EET), in the recent literature. This technique enables the construction of an equilibrated flux field satisfying (9), denoted $\widehat{\boldsymbol{q}}_H^\varepsilon$ in the following, from a post-processing of the MsFEM flux $\boldsymbol{q}_H^\varepsilon = A^\varepsilon \nabla u_H^\varepsilon$ at hand and from the solutions to independent elementary problems. This method, which is an extension to MsFEM of the one exposed in [25] for FEM simulations, is made of two steps:

- **Step 1:** construction of tractions $\widehat{g}_K$ along the edges of each element $K \in \mathcal{T}_H$. These tractions should satisfy the equilibrium at the element level:

$$\forall K, \quad \int_K f + \int_{\partial K} \widehat{g}_K = 0. \tag{11}$$

  We will see below that (11) indeed holds. In order to satisfy the continuity of normal fluxes along element edges, tractions are defined as $\widehat{g}_{K|\Gamma} = \eta_K^\Gamma \widehat{g}_{|\Gamma}$ over each edge Γ of ∂K, with $\eta_K^\Gamma = \pm 1$ and where $\widehat{g}_{|\Gamma}$ has a well-defined value on Γ.

- **Step 2:** local construction of $\widehat{\boldsymbol{q}}_{H|K}^\varepsilon$, over each element $K \in \mathcal{T}_H$, such that

$$-\mathrm{div}\, \widehat{\boldsymbol{q}}_{H|K}^\varepsilon = f \ \text{ in } K, \qquad \widehat{\boldsymbol{q}}_{H|K}^\varepsilon \cdot n_K = \widehat{g}_K \ \text{ on } \partial K, \tag{12}$$

  where $\widehat{g}_K$ are the tractions built in Step 1, and n_K is the outgoing normal on ∂K.

We note that the reconstruction method we use is based on fine-scale computations (Step 2) only at the element level (and not on patches of elements, as for alternative reconstruction methods). It is therefore particularly suited to the MsFEM framework, where fine-scale computations are expensive. We now describe these two steps in more details.

Computation of equilibrated tractions. An arbitrary but convenient manner to derive equilibrated tractions $\widehat{g}_K$ by post-processing $\boldsymbol{q}_H^\varepsilon$ is the enforcement of the so-called *prolongation condition*. We require that, for each element K and each node i connected to K,

$$\int_K (\widehat{\boldsymbol{q}}_H^\varepsilon - \boldsymbol{q}_H^\varepsilon) \cdot \nabla \phi_i^\varepsilon = 0.$$

Since $\widehat{\boldsymbol{q}}_H^\varepsilon \in W$, this is equivalent to requiring that

$$\int_{\partial K} \widehat{g}_K \, \phi_i^\varepsilon = \int_K (\boldsymbol{q}_H^\varepsilon \cdot \nabla \phi_i^\varepsilon - f \, \phi_i^\varepsilon) =: Q_i^K, \tag{13}$$

where $\widehat{g}_K = \widehat{\boldsymbol{q}}_H^\varepsilon \cdot n_K$ on ∂K. Note that the quantity Q_i^K is fully computable. Enforcing (13) naturally provides for the local equilibrium condition (11) due to the partition of unity property.

Collecting the relations (13) for all the elements connected to a given node i yields a local system where the unknowns are the projections $\displaystyle\int_{\partial K} \widehat{g}_K \, \phi_i^\varepsilon$ of the tractions $\widehat{g}_K$ on the basis

function ϕ_i^ε. The local system spreads over the support of ϕ_i^ε, i.e. the patch Ω_i of elements connected to node i. As an example, consider an internal vertex node i connected to N elements in a 2D mesh $\mathcal{T}_H$ made of triangular elements (see Figure 3). Since $\phi^\varepsilon_{i|\partial\Omega_i} = 0$ and ϕ_i^ε is continuous across $\Gamma_{jk} = \partial K_j \cap \partial K_k$, the local system reads

$$\begin{aligned}
\widehat{b}_i^{(1,2)} - \widehat{b}_i^{(N,1)} &= Q_i^{K_1}, \\
\widehat{b}_i^{(2,3)} - \widehat{b}_i^{(1,2)} &= Q_i^{K_2}, \\
\ldots &= \ldots \\
\widehat{b}_i^{(N-1,N)} - \widehat{b}_i^{(N-2,N-1)} &= Q_i^{K_{N-1}}, \\
\widehat{b}_i^{(N,1)} - \widehat{b}_i^{(N-1,N)} &= Q_i^{K_N},
\end{aligned} \tag{14}$$

with $\widehat{b}_i^{(j,k)} = \displaystyle\int_{\Gamma_{jk}} \eta_{K_j}^{\Gamma_{jk}}\, \widehat{g}_{|\Gamma_{jk}}\, \phi_i^\varepsilon$. There are N equations and N unknowns. The $N \times N$ matrix corresponding to the linear system (14) is however not invertible. Solutions to (14) yet exist since the right-hand side of (14) satisfies the appropriate compatibility condition. Uniquely defined $\widehat{b}_i$ may be obtained by minimizing an appropriate cost function over the solutions to (14).

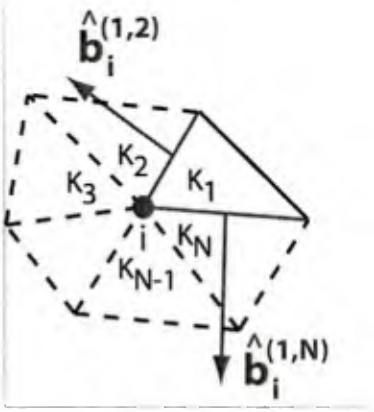

Figure 3: Illustration of the prolongation condition applied to elements connected to a node i in a 2D mesh.

Once projections $\widehat{b}_i^{(j,k)}$ have been obtained for all nodes i of the mesh $\mathcal{T}_H$ and all edges $\Gamma_{jk} \subset \Omega_i$, tractions $\widehat{g}_{\Gamma_{jk}}$ over the edge Γ_{jk} can be recovered. We choose to search $\widehat{g}_{\Gamma_{jk}}$ as an affine combination of the functions $\left\{\phi^\varepsilon_{i|\Gamma_{jk}}\right\}_{1\leq i\leq I}$. For the 2D example of Figure 4, this reads

$$\widehat{g}_{\Gamma_{jk}} = \eta_{K_j}^{\Gamma_{jk}}\, \langle \boldsymbol{q}_H^\varepsilon \rangle_{\Gamma_{jk}} \cdot n_{K_j} + \alpha_1\, \phi^\varepsilon_{i_1|\Gamma_{jk}} + \alpha_2\, \phi^\varepsilon_{i_2|\Gamma_{jk}},$$

where $\langle \boldsymbol{q}_H^\varepsilon \rangle_{\Gamma_{jk}} := \dfrac{1}{2}(\boldsymbol{q}^\varepsilon_{H|K_j} + \boldsymbol{q}^\varepsilon_{H|K_k}) = \dfrac{1}{2}(A^\varepsilon \nabla u^\varepsilon_{H|K_j} + A^\varepsilon \nabla u^\varepsilon_{H|K_k})$ is the average of the MsFEM flux on the edge Γ_{jk} and where the nodes i_1 and i_2 are the two vertices of the edge Γ_{jk} (see Figure 4). Enforcing that $\widehat{b}_i^{(j,k)} = \displaystyle\int_{\Gamma_{jk}} \eta_{K_j}^{\Gamma_{jk}}\, \widehat{g}_{|\Gamma_{jk}}\, \phi_i^\varepsilon$ for $i = i_1$ and $i = i_2$ leads to a simple 2×2 linear system on (α_1, α_2) that can be easily solved.

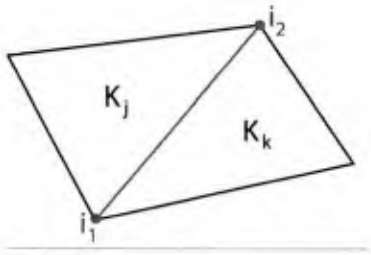

Figure 4: Environment of the interface Γ_{jk}, separating element K_j and element K_k.

Solution to elementary problems. For given tractions $\widehat{g}_K$, the optimal flux field $\widehat{\boldsymbol{q}}$ in the element K is the one that minimizes

$$\left(E_{\mathrm{CRE}|K}(\widehat{u}_H^\varepsilon, \widehat{\boldsymbol{q}})\right)^2 = \int_K (A^\varepsilon)^{-1}(\widehat{\boldsymbol{q}} - A^\varepsilon \nabla \widehat{u}^\varepsilon) \cdot (\widehat{\boldsymbol{q}} - A^\varepsilon \nabla \widehat{u}^\varepsilon)$$

among all flux fields $\widehat{\boldsymbol{q}}$ satisfying (12). This choice indeed makes the upper bound in (10) as small as possible. It can be shown that such fields are given by $\widehat{\boldsymbol{q}}_{H|K}^\varepsilon = A^\varepsilon \nabla w^\varepsilon$, where $w^\varepsilon \in H^1(K)$ is such that

$$\forall v \in H^1(K), \quad B_{|K}^\varepsilon(w^\varepsilon, v) = \int_K f v + \int_{\partial K} \widehat{g}_K \, v, \tag{15}$$

where $B_{|K}^\varepsilon(u,v) = \displaystyle\int_K [A^\varepsilon \nabla u] \cdot \nabla v$. In view of (11), the above local Neumann problem (15) is well-posed (up to the addition of a constant). An accurate approximation $\widetilde{w}^\varepsilon$ of its solution w^ε is in practice computed using a higher-order basis within the element K. In order to reuse the *offline* MsFEM computations at hand and to limit the computational costs, we construct the local higher-order basis using the technique proposed in [16].

In the case when the load f is regular in each element K, computations associated to the resolution of (15) can mostly be performed *offline*, thus avoiding fine-scale computations in the *online* phase, and thus respecting the MsFEM paradigm in multi-query contexts. We refer to [5] for more details.

3.3.3 Adaptive discretization

We have developed above a CRE estimate that yields a fully computable upper bound (10), namely

$$|||u^\varepsilon - u_H^\varepsilon||| \leq E_{\mathrm{CRE}}(u_H^\varepsilon, \widehat{\boldsymbol{q}}_H^\varepsilon) =: \Delta_{\mathrm{MsFEM}} \tag{16}$$

where $\widehat{\boldsymbol{q}}_H^\varepsilon$ is the flux field built in Section 3.3.2. This bound quantifies the overall MsFEM error. As explained in details in [5], it is possible, based on this estimator, to develop error indicators that heuristically assess the various error sources and enable an automatic adaptation of the MsFEM parameters (the coarse mesh size H, the fine mesh size h and the oversampling ratio) in order to reach a given error tolerance while keeping the computational cost minimal. For the sake of brevity, we do not detail this here.

3.4 Numerical results

In this section, we investigate the performances of the proposed methodology on a classical non-periodic problem. The problem is set on $\Omega = (0,1)^2$, with $f = -1$. Dirichlet boundary conditions $u(x) = (x_1 - 0.5)^2 + (x_2 - 0.5)^2$ are applied on $\partial\Omega$. The conductivity properties of the medium are modeled by the matrix

$$A^\varepsilon(x) = \left[2 + P\cos\left(2\pi\tanh(w(r-0.3))/\varepsilon\right)\right] \mathcal{I}_2 = a^\varepsilon(x)\, \mathcal{I}_2,$$

where $r = \sqrt{(x_1 - 0.5)^2 + (x_2 - 0.5)^2}$ is the distance from the center of the fiber. The parameter P controls the contrast in a^ε, the parameter w determines the total width of the reinforcement, and ε sets the wavelength of the unidirectional oscillations. In the following, we set $P = 1.8$, $w = 20$ and $\varepsilon = 0.2$, so that the shortest wavelength in the oscillations is about $\varepsilon_0 = 0.01$. The evolution of a^ε is shown on Figure 5.

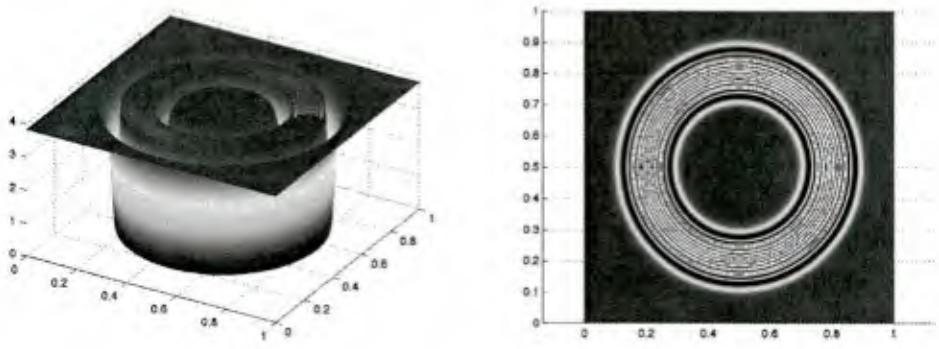

Figure 5: 2D non-periodic example: evolution of a^ε in the domain.

We take an initial coarse mesh $\mathcal{T}_H$ made of 5×5 macro elements. Choosing $h_K = \varepsilon_0/5$ for any K, and with no oversampling, the approximate MsFEM solution is compared to the exact solution (computed using a 500×500 fine mesh) on Figures 6 and 7.

The value of the associated relative error estimate $\Delta_{\text{MsFEM}}/|||u_H^\varepsilon|||$ (where Δ_{MsFEM} is defined by (16)) is about 36%, with an effectivity index of 1.09. Note that, in view of (10), the estimation of the error is always larger than the true error. We observe here that the estimation of the error is only 9% larger than the true error. Local contributions of $(\Delta_{\text{MsFEM}})^2$ over $\mathcal{T}_H$, as well as local effectivity indices, are shown in Figure 8. These local effectivity indices are all between 1.0 and 1.16. The over-estimation of the error is thus limited, and always smaller than 16%. Our procedure to estimate the local error is hence accurate.

We now use the adaptive algorithm from this initial, non-accurate MsFEM solution ($H_K = 0.2$, $h_K = H_K$ and $S_K = K$) and with a prescribed error tolerance of 5%. After a few iterations, this leads to the local MsFEM parameters shown in Figure 9, associated with an estimated error of 4.77%. We observe that this error tolerance can be reached without resorting to accurate fine-scale computations in the center of the domain Ω. Our adaptive algorithm leads to a discretization which is much more efficient than the one that would have been obtained using a uniform refinement.

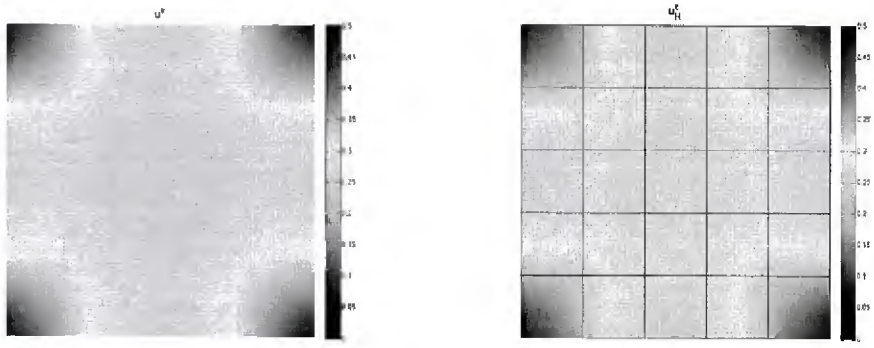

Figure 6: 2D non-periodic example: exact solution u^ε (left) and MsFEM solution u_H^ε (right).

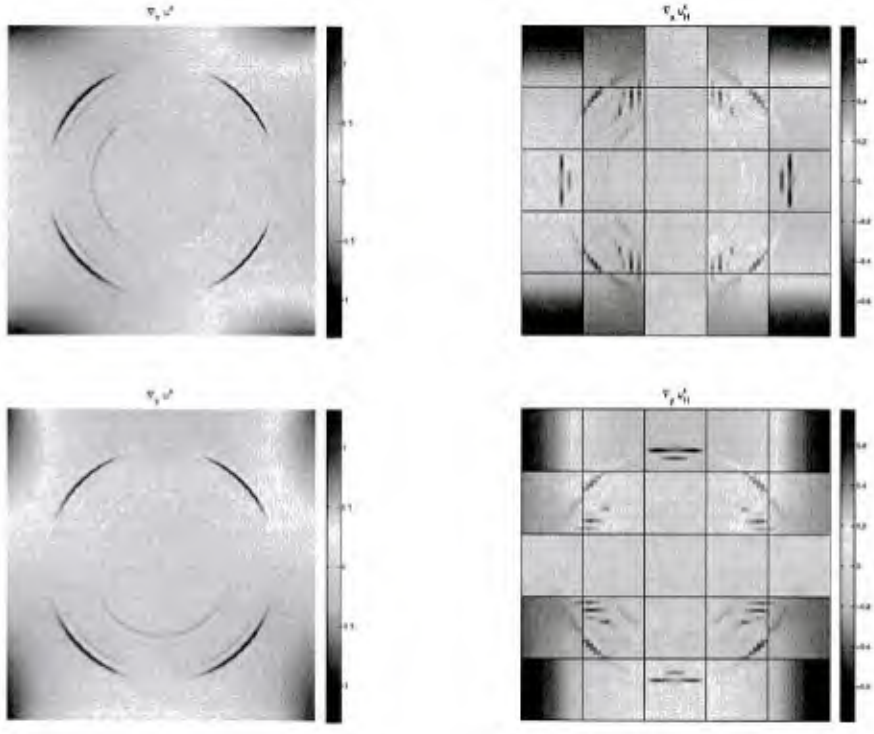

Figure 7: 2D non-periodic example: exact gradient ∇u^ε (left) and MsFEM gradient ∇u_H^ε (right) (top row: components $\nabla u^\varepsilon \cdot e_1$ and $\nabla u_H^\varepsilon \cdot e_1$; bottom row: components $\nabla u^\varepsilon \cdot e_2$ and $\nabla u_H^\varepsilon \cdot e_2$).

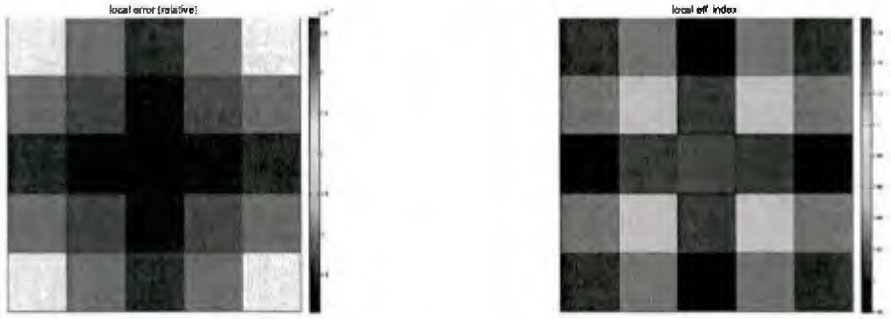

Figure 8: 2D non-periodic example: values of $(\Delta^K_{\mathrm{MsFEM}})^2$ for the specific computed MsFEM solution (left), and local effectivity indices (right).

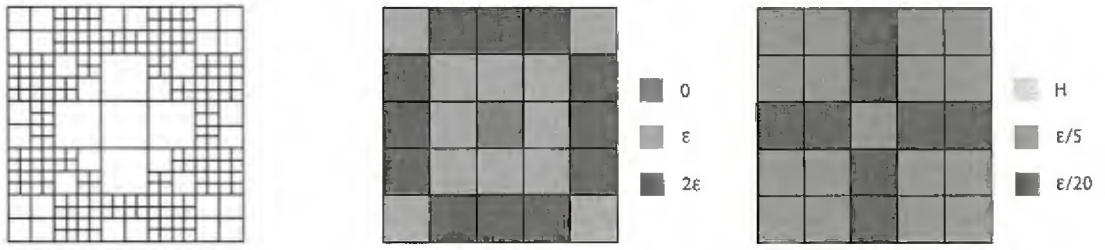

Figure 9: 2D non-periodic example: adapted coarse mesh (left), oversampling size (center) and fine mesh sizes h_K (right).

4 MsFEM approaches for advection dominated problems in perforated domains

[Work expanded in [8]].

The MsFEM approach has initially been introduced for diffusive problems with highly oscillatory coefficients, set on regular domains (see problem (3) for a typical example). With the aim to get a better understanding of the approach, we have considered in some previous works the extension of MsFEM to other problems. First, in [13], we considered the case of a diffusive equation (with constant coefficients) posed on a perforated domain. The multiscale nature of the problem is then encoded in the geometry of the domain on which the equation is posed, rather than in the coefficients of the equation. Starting with [14], we have next considered advection-diffusion problems, which are very relevant equations for the application viewpoint, and which raise several new questions in terms of design of MsFEM approaches. The problem considered in [14] is an advection-diffusion equation, with highly oscillatory coefficients, and posed on a regular domain. In order for this problem to be significantly different (from the theoretical and the numerical standpoints) from a purely diffusive problem, we have considered the regime when advection dominates diffusion. A question of specific interest is whether or not the advection term must be introduced in the equation defining the local basis functions, and whether or not this brings more stability to the approach. The next step, on which we report here, is to consider an advection-diffusion equation, again in the advection-dominated regime, posed on a perforated domain.

We thus consider a regular bounded open set $\Omega \subset \mathbb{R}^d$, in dimension $d \geq 2$, and its subset $\Omega^\varepsilon \subsetneq \Omega$, a domain perforated by holes of presumably small size $\varepsilon > 0$. We denote by $B^\varepsilon = \Omega \setminus \overline{\Omega^\varepsilon}$ the set of perforations (see Figure 10 below). On the perforated domain Ω^ε, we consider the advection-diffusion equation

$$-\alpha \Delta u^\varepsilon + \widehat{b}^\varepsilon \cdot \nabla u^\varepsilon = f \quad \text{in } \Omega^\varepsilon,$$

where $\alpha > 0$, for a right-hand side $f \in L^2(\Omega)$ and for some advection field $\widehat{b}^\varepsilon$. On the outer boundary $\partial\Omega$, we impose homogeneous Dirichlet boundary conditions. On the other hand, the equation can be supplied either with homogeneous Dirichlet or homogeneous Neumann boundary conditions on the boundary of the perforations. More precisely, we concurrently consider in [8] the two problems

$$\left\{ \begin{array}{rcl} -\alpha \Delta u^\varepsilon + \widehat{b}^\varepsilon \cdot \nabla u^\varepsilon &=& f \quad \text{in } \Omega^\varepsilon, \\ u^\varepsilon &=& 0 \quad \text{on } \partial\Omega^\varepsilon, \end{array} \right. \tag{17}$$

and

$$\left\{ \begin{array}{rcl} -\alpha \Delta u^\varepsilon + \widehat{b}^\varepsilon \cdot \nabla u^\varepsilon &=& f \quad \text{in } \Omega^\varepsilon, \\ \alpha \nabla u^\varepsilon \cdot n &=& 0 \quad \text{on } \partial\Omega^\varepsilon \setminus \partial\Omega, \\ u^\varepsilon &=& 0 \quad \text{on } \partial\Omega^\varepsilon \cap \partial\Omega. \end{array} \right. \tag{18}$$

For the sake of brevity, we only discuss here problem (18), and refer to [8] for a comprehensive study of (17).

As pointed out above, we study a regime where advection dominates diffusion. In the absence of perforations, it is well-known that numerical instabilities arise for classical Finite

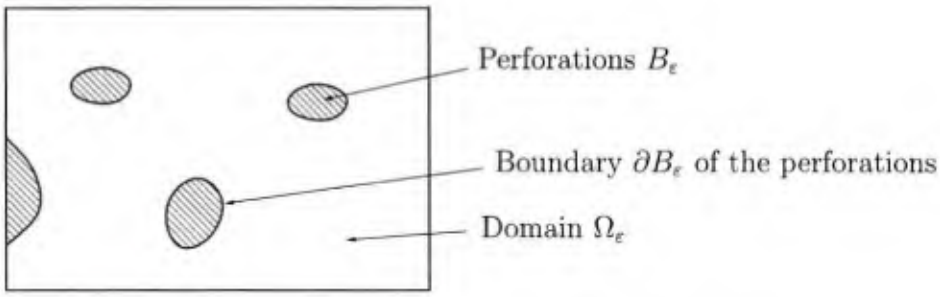

Figure 10: The domain Ω contains perforations B_ε, some of which may intersect $\partial\Omega$. The perforated domain is $\Omega_\varepsilon = \Omega \setminus \overline{B_\varepsilon}$. The boundary of Ω_ε is the union of $\partial B_\varepsilon \cap \overline{\Omega_\varepsilon}$ (the part of the boundary of the perforations that is included in $\overline{\Omega_\varepsilon}$) and of $\partial\Omega \cap \overline{\Omega_\varepsilon}$.

Element methods, and stabilization methods are in order [26]. The case of perforated domains deserves a specific attention, since the perforations are presumably many, and asymptotically infinitely many.

The numerical approaches we consider are variants of the Multiscale Finite Element method (MsFEM). As pointed out in Section 3.2, MsFEM encodes the multiscale character of the problem to be solved in the finite element basis functions by defining the latter as the solutions of independent local problems involving a differential operator identical, or close to that of the original equation (see e.g. [21]). The finite element basis functions are defined independently of the source term and therefore can be precomputed. A Galerkin approximation on the resulting approximation space is then performed. The choice of the boundary conditions imposed on the local problems is a critical issue. In [12], we have introduced Crouzeix-Raviart type boundary conditions for the local problems, in the case of a prototypical diffusion problem. The approach has next been enriched with bubble functions to address the case of the same diffusion equation posed in a perforated domain [13]. The main advantage of this particular choice of Crouzeix-Raviart type boundary conditions has been shown there to be the robustness of the approach with respect to the location of the perforations. The approximation remains accurate, irrespective of the fact that the boundaries of the mesh elements intersect or not the perforations, a sensitive issue for other types of boundary conditions. Since we consider here a problem set on a perforated domain, we again adopt these Crouzeix-Raviart boundary conditions for the MsFEM basis functions.

We first make precise the various numerical approaches we consider in Section 4.1. Under the assumption that the perforations are periodically located, the homogenized limit of (18) is identified in Section 4.2. Our numerical tests, and our conclusions, are presented in Section 4.3. We explore there a periodic test-case (in Section 4.3.1) as well as a non-periodic test-case (in Section 4.3.2). In short, the conclusions for Problem (18) are the following:

- the method using a basis of functions built upon the full advection-diffusion operator enriched with bubble functions built likewise is the best possible approach whatsoever, and it does not require any additional stabilization.
- if one does not wish to include the transport field in the definition of the basis functions, because this might be a difficulty either from the implementation viewpoint or in the context of varying advection fields, then the best to do is to use a stabilized formulation

with basis functions built with the sole diffusive part of the operator, with no enrichment by bubble functions. All other approaches are significantly less efficient.

4.1 Presentation of our numerical approaches

We introduce in this section the different variants of the MsFEM we have considered, that all use Crouzeix-Raviart boundary conditions [12, 13] on the boundary of mesh elements for the definition of the basis functions. We have considered MsFEM approaches that

- use basis functions defined with the full advection-diffusion operator (we abbreviate this into *Adv-MsFEM*), or only the diffusive part of that operator (we abbreviate this into *MsFEM*);
- possibly enrich the approximation space spanned by these functions by adding bubble functions, the latter being either defined with the full advection-diffusion operator, or only the diffusive part of that operator;
- possibly have stabilized variational formulations.

For the discretization, we consider a uniform regular mesh $\mathcal{T}_H$ of Ω with mesh size H. This mesh size is presumably much larger than what would be in order for a classical FEM applied to a problem with small scale ε. We denote by $\mathcal{E}_H^{\text{in}}$ and $\mathcal{E}_H^{\text{ext}}$, respectively, the set of inner and outer edges/faces of the mesh $\mathcal{T}_H$ ($\mathcal{E}_H^{\text{ext}}$ is the set of edges lying in $\partial\Omega$).

The variational formulation of the Neumann problem (18) reads as follows: find $u^\varepsilon \in V$ such that, for any $v \in V$,

$$a(u^\varepsilon, v) = F(v)$$

with

$$a(u,v) = \int_{\Omega^\varepsilon} \alpha \nabla u \cdot \nabla v + \left(\widehat{b}^\varepsilon \cdot \nabla u\right) v \quad \text{and} \quad F(v) = \int_{\Omega^\varepsilon} f\, v$$

and

$$V^\varepsilon = \left\{ u \in H^1(\Omega^\varepsilon) \text{ such that } u = 0 \text{ on } \partial\Omega^\varepsilon \cap \partial\Omega \right\}.$$

The finite dimensional approximation spaces (that we introduce below) are not included in V, since Crouzeix-Raviart boundary conditions allow for discontinuous functions. Our approximations of (18) are therefore not conformal approximations. For the discrete variational formulations, we therefore introduce the following two bilinear forms:

$$a_H(u,v) = \sum_{K \in \mathcal{T}_H} \int_{K \cap \Omega^\varepsilon} \alpha \nabla u \cdot \nabla v + \left(\widehat{b}^\varepsilon \cdot \nabla u\right) v,$$

and

$$a_{\text{diff},H}(u,v) = \sum_{K \in \mathcal{T}_H} \int_{K \cap \Omega^\varepsilon} \alpha \nabla u \cdot \nabla v,$$

which all involve broken integrals.

4.1.1 MsFEM approaches using only the diffusion operator, and their stabilized version

Description of the basis functions. For any $E \in \mathcal{E}_H^{\text{in}}$, we introduce the function $\Phi_0^{\varepsilon,E}$ which is such that, for all mesh elements $K \in \mathcal{T}_H$,

$$\begin{cases} -\alpha\Delta\Phi_0^{\varepsilon,E} = 0 \quad \text{in } K \cap \Omega^\varepsilon, \\ \alpha\nabla\Phi_0^{\varepsilon,E} \cdot n = 0 \quad \text{in } K \cap \partial B^\varepsilon, \\ \text{if } E' \in \mathcal{E}_H^{\text{in}} \cap \partial K, \quad \displaystyle\int_{E' \cap \Omega^\varepsilon} \Phi_0^{\varepsilon,E} = \delta_{E,E'} \quad \text{and} \quad \alpha\nabla\Phi_0^{\varepsilon,E} \cdot n = \lambda^{K,E'} \text{ on } E' \cap \Omega^\varepsilon, \\ \text{if } E' \in \mathcal{E}_H^{\text{ext}} \cap \partial K, \quad \Phi_0^{\varepsilon,E} = 0 \quad \text{on } E' \cap \Omega^\varepsilon, \end{cases} \tag{19}$$

where $\lambda^{K,E'}$ is constant. The function $\Phi_0^{\varepsilon,E}$ is supported in the elements K for which $E \subset \partial K$ (see Figure 11).

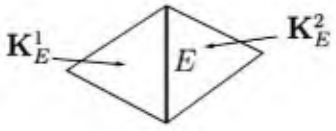

Figure 11: Construction of $\Phi_0^{\varepsilon,E}$ following (19).

We also define, for $K \in \mathcal{T}_H$, the bubble function $\Psi_0^{\varepsilon,K}$, the support of which is reduced to $K \cap \Omega^\varepsilon$, as the solution to

$$\begin{cases} -\alpha\Delta\Psi_0^{\varepsilon,K} = 1 \quad \text{in } K \cap \Omega^\varepsilon, \\ \alpha\nabla\Psi_0^{\varepsilon,K} \cdot n = 0 \quad \text{in } K \cap \partial B^\varepsilon, \\ \text{if } E' \in \mathcal{E}_H^{\text{in}} \cap \partial K, \quad \displaystyle\int_{E' \cap \Omega^\varepsilon} \Psi_0^{\varepsilon,K} = 0 \quad \text{and} \quad \alpha\nabla\Psi_0^{\varepsilon,K} \cdot n = \mu^{K,E'} \text{ on } E' \cap \Omega^\varepsilon, \\ \text{if } E' \in \mathcal{E}_H^{\text{ext}} \cap \partial K, \quad \Psi_0^{\varepsilon,K} = 0 \quad \text{on } E' \cap \Omega^\varepsilon, \end{cases}$$

where $\mu^{K,E'}$ is constant.

We then define the approximation spaces by

$$V_H = \text{Span}\left\{\Phi_0^{\varepsilon,E}, \quad E \in \mathcal{E}_H^{\text{in}}\right\}$$

and

$$V_{H,\text{bubble}} = \text{Span}\left\{\Phi_0^{\varepsilon,E}, \ \Psi_0^{\varepsilon,K}, \quad E \in \mathcal{E}_H^{\text{in}}, \ K \in \mathcal{T}_H\right\}.$$

Variational formulations. The variational formulation of the standard MsFEM approach reads as

$$\text{Find } u_H \in V_H \text{ such that, for any } v_H \in V_H, \quad a_H(u_H, v_H) = F(v_H), \tag{20}$$

while the variational formulation for the variant using bubble functions is

$$\begin{cases} \text{Find } u_H \in V_{H,\text{bubble}} \text{ such that,} \\ \text{for any } v_H \in V_{H,\text{bubble}}, \quad a_H(u_H, v_H) = F(v_H). \end{cases} \tag{21}$$

The stabilized version of (21) (or, *mutatis mutandis*, of (20)) that we use reads as

$$\left\{\begin{array}{l} \text{Find } u_H \in V_{H,\text{bubble}} \text{ such that, for any } v_H \in V_{H,\text{bubble}}, \\ a_H(u_H, v_H) + a_{\text{stab}}(u_H, v_H) = F(v_H) + F_{\text{stab}}(v_H), \end{array}\right. \tag{22}$$

where the stabilization terms are defined by

$$\begin{aligned} a_{\text{stab}}(u_H, v_H) &= \sum_{K \in \mathcal{T}_H} \left(\tau_{\mathbf{K}} \left(-\alpha \Delta u_H + \widehat{b}^\varepsilon \cdot \nabla u_H\right), \widehat{b}^\varepsilon \cdot \nabla v_H\right)_{L^2(K \cap \Omega^\varepsilon)}, \\ F_{\text{stab}}(v_H) &= \sum_{K \in \mathcal{T}_H} \left(\tau_{\mathbf{K}} f, \widehat{b}^\varepsilon \cdot \nabla v_H\right)_{L^2(K \cap \Omega^\varepsilon)}; \end{aligned} \tag{23}$$

with $\tau_{\mathbf{K}}(x) = \dfrac{H}{2\left|\widehat{b}^\varepsilon(x)\right|}\left[\coth\left(\dfrac{\left|\widehat{b}^\varepsilon(x)\right| H}{2\alpha}\right) - \dfrac{2\alpha}{\left|\widehat{b}^\varepsilon(x)\right| H}\right]$. In the case when $\operatorname{div} \widehat{b}^\varepsilon = 0$, the skew-symmetric part of the operator $\mathcal{L}v = -\alpha\Delta v + \widehat{b}^\varepsilon \cdot \nabla v$ is $\mathcal{L}_{\text{ss}} v = \widehat{b}^\varepsilon \cdot \nabla v$ and thus (23) corresponds to a SUPG stabilization.

Details on the stabilized formulations. Given the above basis functions, we can obtain a simpler expression of the term (23) by decomposing $u_H \in V_{H,\text{bubble}}$ as

$$u_H = \sum_{E \in \mathcal{E}_H^{\text{in}}} U_H^E \, \Phi_0^{\varepsilon,E} + \sum_{K \in \mathcal{T}_H} U_H^K \, \Psi_0^{\varepsilon,K}.$$

Following the definition of the basis functions, we have

$$\begin{aligned} a_{\text{stab}}(u_H, v_H) = \sum_{K \in \mathcal{T}_H} \left(\tau_{\mathbf{K}} \left(\widehat{b}^\varepsilon \cdot \nabla u_H\right), \widehat{b}^\varepsilon \cdot \nabla v_H\right)_{L^2(K \cap \Omega^\varepsilon)} \\ + \sum_{K \in \mathcal{T}_H} U_H^K \int_{K \cap \Omega^\varepsilon} \tau_{\mathbf{K}} \left(\widehat{b}^\varepsilon \cdot \nabla v_H\right). \end{aligned} \tag{24}$$

In practice, we make use of a discrete approximation of the basis functions on a fine mesh K_h, and (23) may not be defined in general. For example, if we use a $\mathbb{P}^1$ approximation on a fine mesh K_h for the local problems, then $\nabla u_{H,h}$ may be discontinuous at the interfaces of K_h. As a consequence, we have that

$$-\Delta u_{H,h} \notin L^2(K \cap \Omega^\varepsilon)$$

and the stabilization term (23) has no natural expression when we work with the discretized approximation space $(V_{H,\text{bubble}})_h$ rather than $V_{H,\text{bubble}}$.

To circumvent this difficulty, we use the stabilization term (24) rather than (23). In contrast to (23), the quantity (24) is also well defined on $(V_{H,\text{bubble}})_h$. We point out that this stabilization approach is not strongly consistent. We however note that we have already used (for the same reasons as here) this type of non-strongly consistent stabilization approach in [14], where we were able to show the convergence of the approach (see [14, Section 3.2]).

4.1.2 MsFEM approaches using the full advection-diffusion operator, and their stabilized version

In this variant, we use basis functions that depend on the advection field.

Description of the basis functions. For any $E \in \mathcal{E}_H^{\rm in}$, the function $\Phi_{\rm N}^{\varepsilon,E}$ is defined by

$$\begin{cases} -\alpha\Delta\Phi_{\rm N}^{\varepsilon,E} + \widehat{b}^{\varepsilon}\cdot\nabla\Phi_{\rm N}^{\varepsilon,E} = 0 \quad \text{in } K\cap\Omega^{\varepsilon}, \\ \left(\alpha\nabla\Phi_{\rm N}^{\varepsilon,E}\right)\cdot n = 0 \quad \text{in } K\cap\partial B^{\varepsilon}, \\ \text{if } E'\in\mathcal{E}_H^{\rm in}\cap\partial K, \quad \displaystyle\int_{E'\cap\Omega^{\varepsilon}}\Phi_{\rm N}^{\varepsilon,E} = \delta_{E,E'} \\ \qquad\qquad \text{and} \quad \left(\alpha\nabla\Phi_{\rm N}^{\varepsilon,E}\right)\cdot n = \lambda^{K,E'} \text{ on } E'\cap\Omega^{\varepsilon}, \\ \text{if } E'\in\mathcal{E}_H^{\rm ext}\cap\partial K, \quad \Phi_{\rm N}^{\varepsilon,E} = 0 \quad \text{on } E'\cap\Omega^{\varepsilon}, \end{cases}$$

while the bubble function $\Psi_{\rm N}^{\varepsilon,K}$ is the solution to

$$\begin{cases} -\alpha\Delta\Psi_{\rm N}^{\varepsilon,K} + \widehat{b}^{\varepsilon}\cdot\nabla\Psi_{\rm N}^{\varepsilon,K} = 1 \quad \text{in } K\cap\Omega^{\varepsilon}, \\ \left(\alpha\nabla\Psi_{\rm N}^{\varepsilon,K}\right)\cdot n = 0 \quad \text{in } K\cap\partial B^{\varepsilon}, \\ \text{if } E'\in\mathcal{E}_H^{\rm in}\cap\partial K, \quad \displaystyle\int_{E'\cap\Omega^{\varepsilon}}\Psi_{\rm N}^{\varepsilon,K} = 0 \\ \qquad\qquad \text{and} \quad \left(\alpha\nabla\Psi_{\rm N}^{\varepsilon,K}\right)\cdot n = \mu^{K,E'} \quad \text{on } E'\cap\Omega^{\varepsilon}, \\ \text{if } E'\in\mathcal{E}_H^{\rm ext}\cap\partial K, \quad \Psi_{\rm N}^{\varepsilon,K} = 0 \quad \text{on } E'\cap\Omega^{\varepsilon}, \end{cases}$$

where $\lambda^{K,E'}$ and $\mu^{K,E'}$ are constant.

We then introduce the approximation spaces

$$V_H^{\rm adv} = \text{Span}\left\{\Phi_{\rm N}^{\varepsilon,E}, \quad E\in\mathcal{E}_H^{\rm in}\right\}$$

and

$$V_H^{\text{adv bubble}} = \text{Span}\left\{\Phi_{\rm N}^{\varepsilon,E},\ \Psi_{\rm N}^{\varepsilon,K}, \quad E\in\mathcal{E}_H^{\rm in},\ K\in\mathcal{T}_H\right\}.$$

Variational formulations. When no bubble functions are used to enrich the approximation space, the variational formulation reads as

$$\text{Find } u_H\in V_H^{\rm adv} \text{ such that, for any } v_H\in V_H^{\rm adv}, \quad a_H(u_H,v_H) = F(v_H). \tag{25}$$

When using bubble functions, we consider the variational formulation

$$\begin{cases} \text{Find } u_H\in V_H^{\text{adv bubble}} \text{ such that,} \\ \text{for any } v_H\in V_H^{\text{adv bubble}}, \quad a_H(u_H,v_H) = F(v_H). \end{cases} \tag{26}$$

The stabilized version of the formulation (26) reads as

$$\begin{cases} \text{Find } u_H\in V_H^{\text{adv bubble}} \text{ such that, for any } v_H\in V_H^{\text{adv bubble}}, \\ a_H(u_H,v_H) + a_{\rm stab}(u_H,v_H) = F(v_H) + F_{\rm stab}(v_H). \end{cases} \tag{27}$$

For the same reasons as those for which we favor (24) over (23), we choose the stabilization defined by

$$a_{\text{stab}}(u_H, v_H) = \sum_{K \in \mathcal{T}_H} U_H^K \int_{K \cap \Omega^\varepsilon} \tau_{\mathbf{K}} \left(\widehat{b}^\varepsilon \cdot \nabla v_H \right). \tag{28}$$

Note that, for the formulation (25), the stabilization is void as $a_{\text{stab}}(u_H, v_H) = 0$ for any $u_H \in V_H^{\text{adv}}$.

4.2 Homogenization results

In this section 4.2, we consider periodic perforations. More precisely, let $Y = (0,1)^d$ be the unit square and $\mathcal{O} \subset Y$ be some smooth perforation (by simplicity, we denote $\mathcal{O}$ *a perforation*, although $\mathcal{O}$ may be the union of several disconnected sets). We scale $\mathcal{O}$ and Y by a factor ε and then periodically repeat this pattern with periods ε in all directions. The set of perforations is therefore

$$B_\varepsilon = \Omega \cap (\cup_{k \in \mathbb{Z}^d} \varepsilon B_k) \quad \text{with} \quad B_k = k + \mathcal{O} \tag{29}$$

and the perforated domain is $\Omega_\varepsilon = \Omega \setminus \overline{B_\varepsilon}$. We also introduce

$$\mathcal{P} = \cup_{k \in \mathbb{Z}^d} \left(k + Y \setminus \overline{\mathcal{O}} \right).$$

For the convenience of the reader, we include here some results of homogenization for (18). These results are useful to bear in mind the asymptotic behavior of the solution u^ε we approximate. The proofs of these results are essentially contained in the literature (we refer e.g. to the textbook [24]).

In Theorem 1, we consider the case when

$$\text{div } b \leq 0 \ \text{ in } \ Y \setminus \overline{\mathcal{O}} \qquad \text{and} \qquad b \cdot n \geq 0 \ \text{ on } \ \partial\mathcal{O}. \tag{30}$$

Since b is periodic, the assumption (30) is equivalent to the assumption

$$\text{div } b = 0 \text{ in } Y \setminus \overline{\mathcal{O}} \quad \text{and} \quad b \cdot n = 0 \text{ on } \partial\mathcal{O}. \tag{31}$$

Theorem 1 *We assume* (29), *that* $\overline{\mathcal{O}} \subset Y$ *and that* $Y \setminus \overline{\mathcal{O}}$ *is a connected open set of* $\mathbb{R}^d$. *We also assume that, uniformly in* ε, *we have* $H^1(\Omega^\varepsilon) \hookrightarrow H^{1/2}(\partial\Omega^\varepsilon)$, *i.e. there exists some* C *independent of* ε *such that*

$$\forall v \in H^1(\Omega^\varepsilon), \qquad \|v\|_{H^{1/2}(\partial\Omega^\varepsilon)} \leq C \|v\|_{H^1(\Omega^\varepsilon)}. \tag{32}$$

Let $\widehat{b}^\varepsilon = b\left(\frac{\cdot}{\varepsilon}\right)$ *where* b *belongs to* $(W^{1,p}(Y \setminus \overline{\mathcal{O}}))^d$ *for some* $p > d$, *is* Y*-periodic and satisfies* (30) *(i.e.* (31)*). We assume that* $f \in L^2(\Omega)$.

Then Problem (18) *is well-posed and its solution* u^ε *satisfies*

$$\lim_{\varepsilon \to 0} \left\| u^\varepsilon - u^\star - \varepsilon \sum_{i=1}^d w_i\left(\frac{\cdot}{\varepsilon}\right) \partial_{x_i} u^\star \right\|_{H^1(\Omega^\varepsilon)} = 0,$$

where $u^\star$ is the solution to the problem

$$\begin{cases} -\text{div}\,(A^\star \nabla u^\star) + b^\star \cdot \nabla u^\star = \dfrac{|Y \setminus \overline{\mathcal{O}}|}{|Y|} f \quad \text{in } \Omega, \\ u^\star = 0 \quad \text{on } \partial\Omega, \end{cases} \tag{33}$$

where the matrix $A^\star$ and the vector $b^\star$ are constant and given, for $1 \leq i \leq d$, by

$$A^\star\, e_i = \frac{1}{|Y|} \int_{Y \setminus \overline{\mathcal{O}}} \alpha \left(e_i + \nabla w_i\right), \qquad b^\star \cdot e_i = \frac{1}{|Y|} \int_{Y \setminus \overline{\mathcal{O}}} b \cdot (e_i + \nabla w_i), \tag{34}$$

and where w_i is the solution to the cell problem

$$\begin{cases} -\Delta w_i = 0 \quad \text{in } \mathcal{P}, \\ w_i \text{ is } Y\text{-periodic}, \quad (\nabla w_i + e_i) \cdot n = 0 \text{ on } \partial\mathcal{O}. \end{cases} \tag{35}$$

Note that (34) also reads $b^\star = \dfrac{1}{|Y|} \displaystyle\int_{Y \setminus \overline{\mathcal{O}}} b$. The assumption (32) amounts to a geometrical assumption on the perforations that intersect the boundary of Ω (see Figure 12).

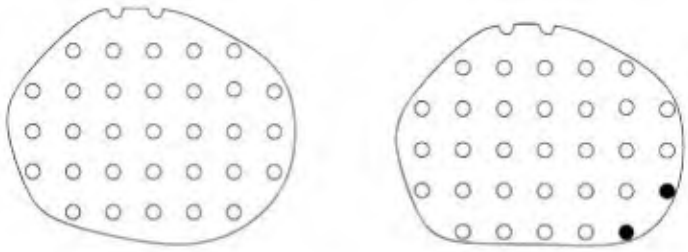

Figure 12: Left: a situation when (32) holds. Right: a situation when (32) does not hold (the boundary $\partial\Omega$ is tangent to the boundary of some perforations, including those shown in black; the domain Ω^ε is thus singular).

We next address in Theorem 2 the case of a general advection field b.

Theorem 2 *We make the same assumptions as for Theorem 1, except that here b does not satisfy* (30) *or* (31). *Then Problem* (18) *is well-posed and its solution u^ε satisfies*

$$\lim_{\varepsilon \to 0} \left\| u^\varepsilon - u^\star - \varepsilon \sum_{i=1}^{d} w_i \left(\frac{\cdot}{\varepsilon}\right) \partial_{x_i} u^\star \right\|_{H^1(\Omega^\varepsilon)} = 0,$$

where $u^\star$ is the solution to (33) *and w_i is the solution to the cell problem* (35). *In the homogenized problem* (33), *the matrix $A^\star$ and the vector $b^\star$ are constant and given by* (34).

The proof of Theorem 1 uses the fact that b is divergence-free, while the proof of Theorem 2 amounts to showing that one can get back to a situation where (30), and thus (31), holds.

4.3 Numerical results

This section presents our numerical results. We consider the two-dimensional domain $\Omega = (0,1)^2$. In Section 4.3.1, its subdomain Ω^ε is a periodically perforated domain defined by

$$\Omega^\varepsilon = \left\{ x \in \Omega, \quad \chi\left(\frac{x}{\varepsilon}\right) = 1 \right\}, \tag{36}$$

where χ is the extension by $\mathbb{Z}^d$-periodicity of the characteristic function $1_{Y\setminus\overline{\mathcal{O}}}$, where $\mathcal{O} \subset Y$ defines a perforation. In Section 4.3.2, we consider non-periodic perforations.

For either of our approaches (based on the diffusion operator only or the full advection-diffusion operator), we investigate several issues. The first issue is how enriching the approach with bubble functions affects the accuracy. Of course, this enrichment comes at the price of increasing the number of degrees of freedom. We observe that the gain in accuracy is much higher than that obtained by, say, reducing the size of the coarse mesh by a factor two. Other issues are the influence of the Péclet number (measuring the relative amplitude of the advection with respect to the diffusion) and that of the small scale ε defining both the size of the perforations and their typical distance.

Beside comparing the various approaches considered, and assessing their performance in function of the various parameters of the problem, we also specifically assess their robustness with respect to the location of the perforations. To this aim, we consider two locations for the perforation within the periodic cell $Y = (0,1)^2$:

$$\mathcal{O} = \mathcal{O}_1 = (0.25, 0.75)^2$$

and

$$\mathcal{O} = \mathcal{O}_2 = (0, 0.25) \times (0.25, 0.75) \cup (0.75, 1) \times (0.25, 0.75).$$

The shape of the perforations is the same (squares of size 0.5ε). The difference lies in the relative position of the mesh with respect to the perforations (see Figure 13). One set of perforations is obtained from the other by shifting the perforations by $0.5\,\varepsilon$ in the x direction. When $\mathcal{O} = \mathcal{O}_1$, the perforations do not intersect the edges of the mesh elements (which are taken aligned with the periodic cells). In contrast, when $\mathcal{O} = \mathcal{O}_2$, many edges are intersected by the perforations. In doing so, we have in mind, like in our previous work [13], to use these two specific periodic geometries to emphasize which approaches can easily carry over to the case of non-periodic perforations (such as the one considered in Section 4.3.2), where a typical mesh may often intersect the perforations. To some extent, the two periodic geometries we consider respectively represent the best case scenario (when perforations are all interior to mesh elements) and the worst case scenario (when "half" the perforations intersect the boundaries of mesh elements).

In all what follows, the advection field $\widehat{b^\varepsilon}$ is equal to the constant field $b = (1,1)^T$, and we choose $f(x,y) = \sin\left(\frac{\pi}{2}x\right)\sin\left(\frac{\pi}{2}y\right)$ as right-hand side (we have checked that our results and conclusions do not sensitively depend on the choice of f).

The reference solution u_{ref}, and all the relative errors that are defined with respect to that reference solution, are computed on the fine mesh. The reference solution itself is computed using the standard $\mathbb{P}^1$ Finite Element method on this fine mesh. We measure the accuracy

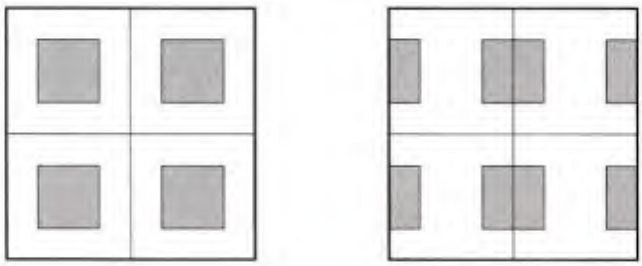

Figure 13: Representation of one coarse element in dimension 2 (of size $H \times H$) containing 4 periodic cells (we assume on this figure that $\varepsilon = H/2$). Perforations are represented in grey. Left: the perforation $\mathcal{O}_1$ does not intersect the mesh edges. Right: the perforation $\mathcal{O}_2$ intersects some mesh edges.

using, on domains $\omega \subset \Omega^\varepsilon$, the H^1 broken norm

$$|u|_{H^1_H(\omega)} = \left(\sum_{K \in \mathcal{T}_H} \|\nabla u\|^2_{L^2(K \cap \omega)} \right)^{1/2}, \tag{37}$$

and the relative errors

$$e_{H^1(\omega)}(u) = \frac{|u - u_{\text{ref}}|_{H^1_H(\omega)}}{|u_{\text{ref}}|_{H^1(\omega)}}, \tag{38}$$

in the *whole* domain ($\omega = \Omega^\varepsilon$) and, possibly, separately inside and outside the boundary layer when there is such a boundary layer close to some portion of the boundary of the domain Ω.

4.3.1 A periodic case

As announced above, the method of preference is a classical, non-stabilized approach using a basis of functions built upon the full advection-diffusion operator enriched with bubble functions built likewise (namely, the "Adv-MsFEM + adv Bubbles" approach). If, for some reason, one does not wish to include the transport field in the definition of the basis functions, then there is an alternate possibility. The best to do is to use a stabilized formulation with basis functions built with the sole diffusive part of the operator (that is, the "Stab-MsFEM" approach). All other approaches turn out to be significantly less efficient.

As expressed by Theorem 2, the homogenized problem is an advection-dominated problem posed in Ω. It has to comply with the Dirichlet boundary conditions on the outer boundary of the domain Ω. Given the orientation of $\widehat{b}^\varepsilon$, a boundary layer is expected close to the upper right corner of Ω. We denote by $\Omega_{\text{layer}} = \Big((0,1)\times(1-\delta_{\text{layer}},1)\Big) \cup \Big((1-\delta_{\text{layer}},1)\times(0,1)\Big)$ this expected boundary layer, of approximate width $\delta_{\text{layer}} = \dfrac{1}{\text{Pe}}\log(\text{Pe})$, with $\text{Pe} = \left\|\widehat{b}^\varepsilon\right\|_{L^\infty(\Omega^\varepsilon)} / (2\alpha)$.

Influence of the Péclet number. We investigate here how the approaches perform when advection increasingly dominates diffusion. In practice, we perform our tests fixing $\varepsilon = 0.03125$, $H = 1/16$ and varying $\alpha = 2^k$, for integers $k = -9$ to -2.

It is well known that all discretization methods (including ours) poorly perform within the boundary layer in the advection dominated regime. Therefore, in order to discriminate

between the approaches, we only consider the region outside the boundary layer. Figure 14 shows the relative error (38) (for $\omega = \Omega^\varepsilon \setminus \Omega_{\text{layer}}$ in (37)) calculated there, in the configuration where the perforations do not intersect the coarse mesh, i.e. when $\mathcal{O} = \mathcal{O}_1$. We observe that Adv-MsFEM performs well. As is the case for MsFEM, provided it is stabilized. Figure 15 shows the results of the same tests for $\mathcal{O} = \mathcal{O}_2$. It confirms the same conclusions, qualitatively, and therefore the flexibility of our approaches all based upon Crouzeix-Raviart type boundary conditions.

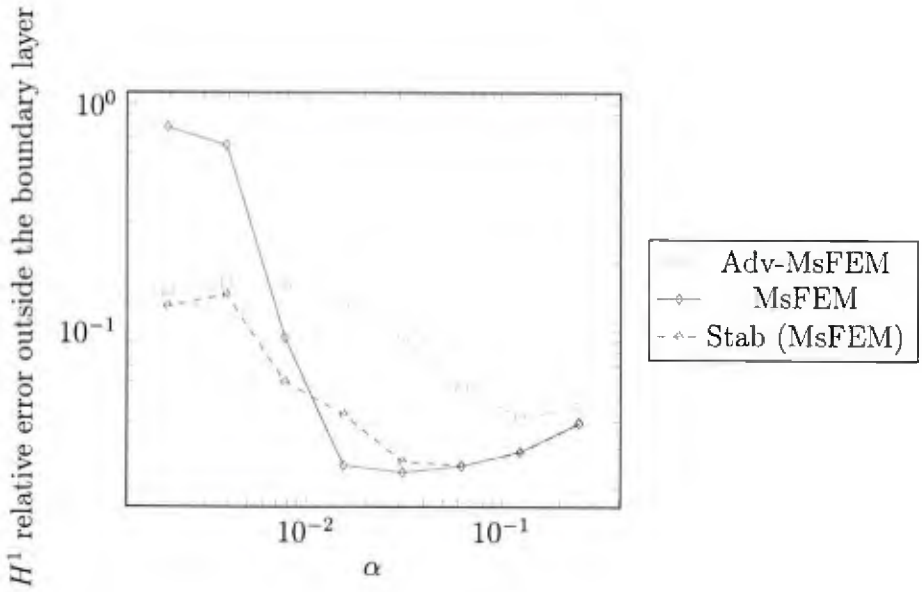

Figure 14: [Neumann Problem (18)] Sensitivity to the Péclet number: error outside the boundary layer when $\mathcal{O} = \mathcal{O}_1$.

Influence of the small scale ε. We fix $\alpha = 1/256$, $H = 1/16$ and we vary $\varepsilon = 2^{-k}$, $k = 5, \ldots, 8$. We only show here the results when the perforations do not intersect the coarse mesh, i.e. when $\mathcal{O} = \mathcal{O}_1$. The results for $\mathcal{O} = \mathcal{O}_2$ are similar (results not shown).

Figures 16 and 17 both show that the relative error, respectively throughout the domain and outside the boundary layer, is essentially insensitive to the small scale ε. The comparison of the actual size of the error in each of the two figures shows that the error within the boundary layer significantly dominates that outside the layer and is often prohibitively large, as is usually the case in the advection-dominated regime. In both figures, we observe that MsFEM is outperformed. Overall, Adv-MsFEM performs the best, but Stab-MsFEM is the most accurate method outside the boundary layer.

Adding bubble functions. We now study the added value of bubble functions for Adv-MsFEM and, given the above conclusions that show the inaccuracy of MsFEM itself, for the stabilized variant Stab-MsFEM.

We first consider the Adv-MsFEM with advective bubble functions, and investigate the influence of the Péclet number. Figure 18 displays the relative H^1 broken error of our different

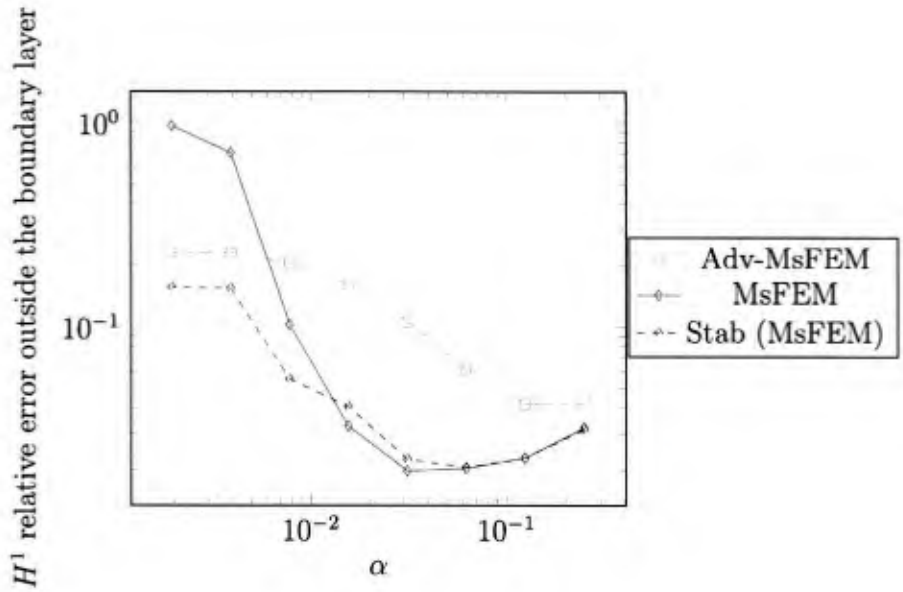

Figure 15: [Neumann Problem (18)] Sensitivity to the Péclet number: error outside the boundary layer when $\mathcal{O} = \mathcal{O}_2$.

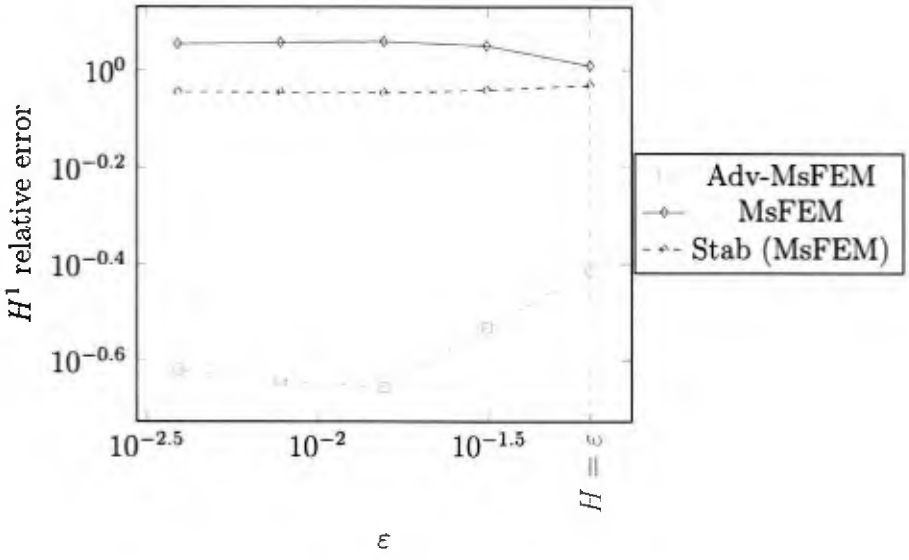

Figure 16: [Neumann Problem (18)] Sensitivity to the small scale ε: error in the whole domain.

approaches outside the boundary layer, when $\mathcal{O} = \mathcal{O}_1$. The conclusions for the case $\mathcal{O} = \mathcal{O}_2$ (results not shown) are similar. We observe that the Adv-MsFEM with advective bubble functions outperforms the Adv-MsFEM and the Stab-MsFEM (without bubble functions).

For the sake of completeness, we briefly discuss the qualitative features of the reference and numerical solutions. Figure 19 shows the fine mesh we use to compute the reference solution

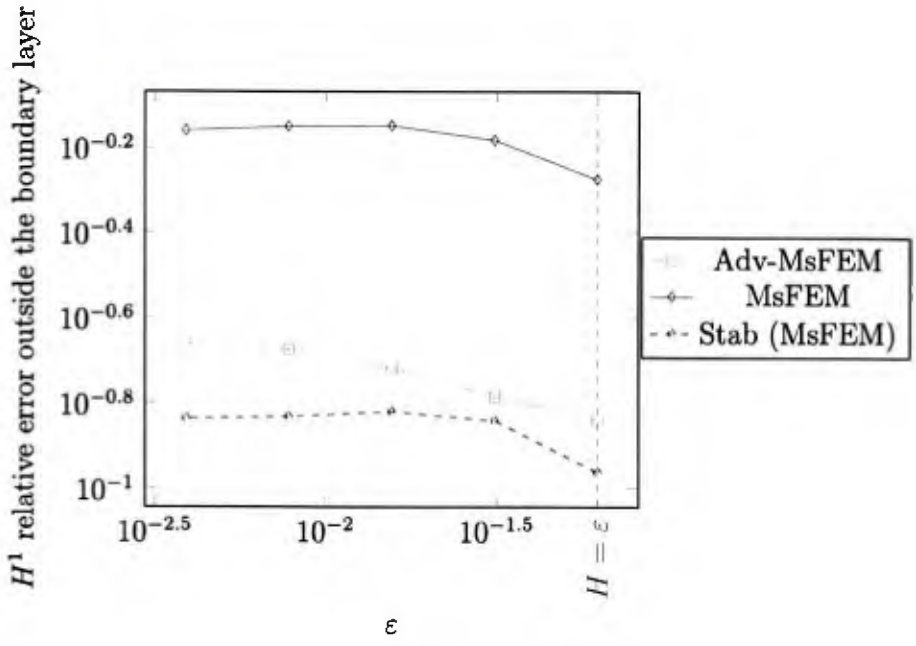

Figure 17: [Neumann Problem (18)] Sensitivity to the small scale ε: error outside the boundary layer.

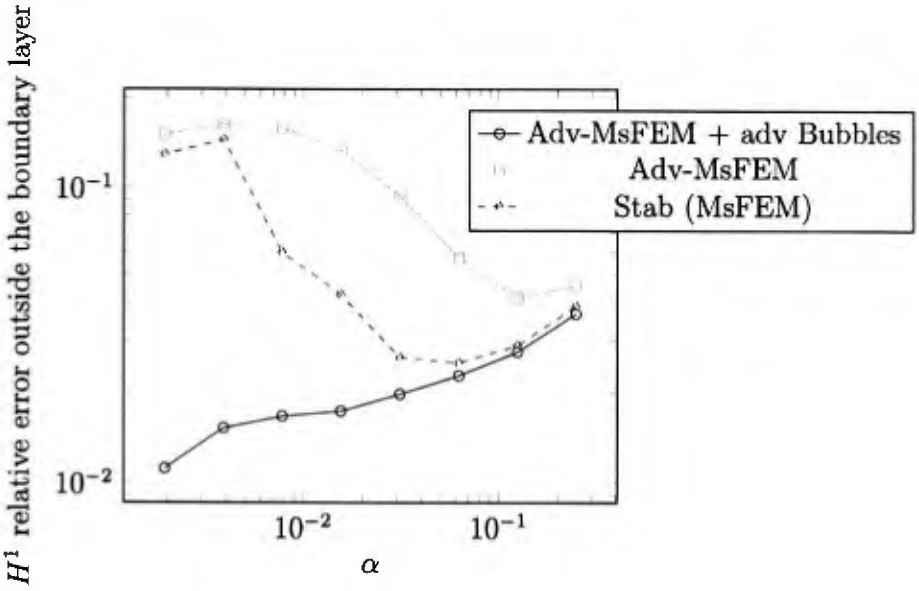

Figure 18: [Neumann Problem (18)] Adding bubble functions: error outside the boundary layer.

and the MsFEM basis functions, along with the reference solution, in the case $\alpha = 1/256$ and $\mathcal{O} = \mathcal{O}_1$. Recall that the advection field is $\widehat{b}^\varepsilon = (1,1)^T$. The advection dominates diffusion,

and a boundary layer can be seen close to the top right corner of the domain (see top of Figure 20, where we show the reference solution close to that corner, in the cases $\alpha = 1/256$ and $\alpha = 1/512$, again in the case $\mathcal{O} = \mathcal{O}_1$). Its width is much smaller than H (however, the fine mesh size h is chosen to be very small, in order to resolve the boundary layer). As expected, the smaller α is, the thiner the boundary layer is. The reference solution hence shows the usual qualitative aspects encountered in advection-dominated problems. Despite the difficulty of this test-case, our "Adv-MsFEM + adv Bubbles" approach performs very well. The error is small (see Figure 18), and is essentially uniformly distributed over the domain Ω^ε (see bottom of Figure 20).

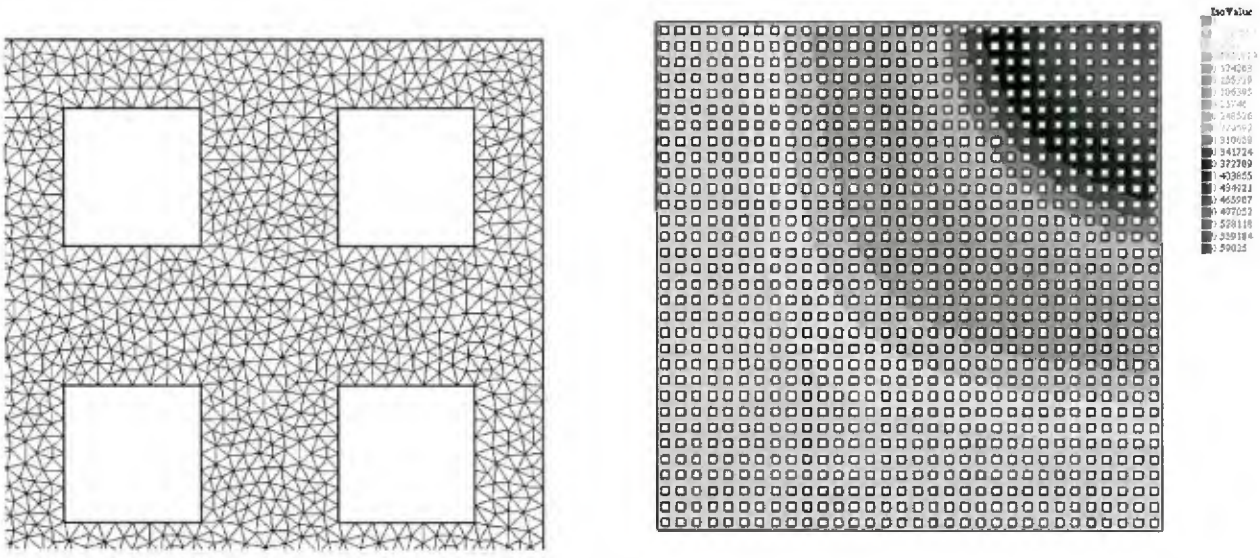

Figure 19: Left: fine mesh used to compute the reference solution and the MsFEM basis functions ($H = 1/16$, $\varepsilon = 1/32$, $h = 1/512$). Only the mesh close to the top right corner of Ω is shown. Right: reference solution for $\alpha = 1/256$ over Ω^ε.

We next investigate the influence of the small scale ε. In Figure 21, we observe, for $\mathcal{O} = \mathcal{O}_1$, that the Adv-MsFEM with advective bubble functions yields a reasonable accuracy. Choosing next $\mathcal{O} = \mathcal{O}_2$, we see on Figure 22 the relative H^1 broken error of the Adv-MsFEM with advective bubble functions inside and outside the boundary layer. Comparing Figures 21 and 22, we infer that:

- inside the boundary layer, the Adv-MsFEM with advective bubble functions is sensitive to the location of the perforations with respect to the coarse mesh;
- outside the boundary layer, the Adv-MsFEM with advective bubble functions is robust to the location of the perforations with respect to the coarse mesh.

Second, we turn to the case of Stab-MsFEM with bubble functions. We investigate the influence of the Péclet number in the case $\mathcal{O} = \mathcal{O}_1$. Figure 23 shows the error outside the boundary layer. We observe that adding bubble functions (either computed with the diffusive part of the operator or the full advection-diffusion operator) does not improve the accuracy

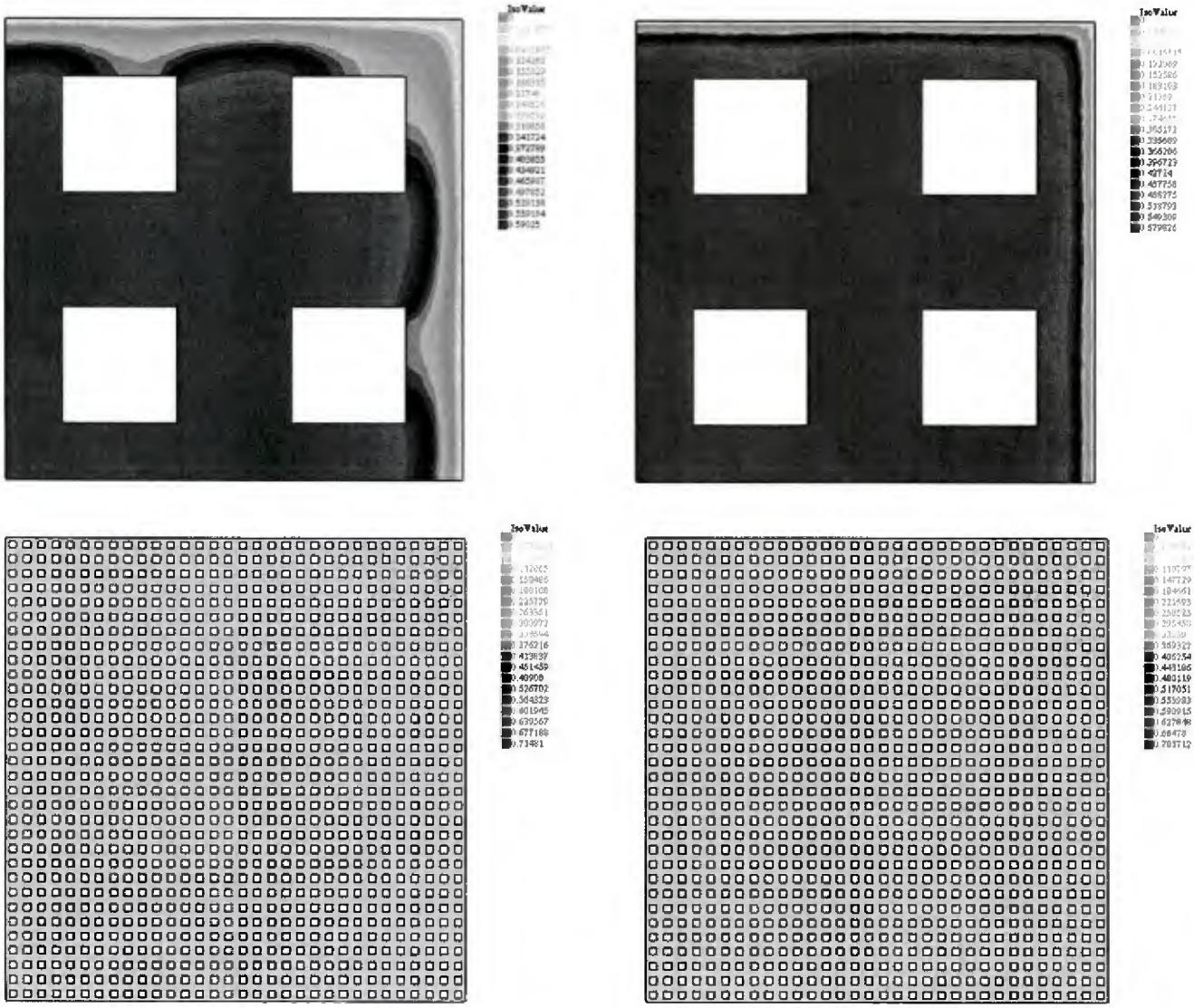

Figure 20: Top: reference solution for $\alpha = 1/256$ (left) and $\alpha = 1/512$ (right). In both cases, we only show the region close to the top right corner of Ω. Bottom: error over Ω^ε between the reference solution and the "Adv-MsFEM + adv Bubbles" solution (computed with $H = 1/16$, $\varepsilon = 1/32$ and $h = 1/512$) for $\alpha = 1/256$ (left) and $\alpha = 1/512$ (right).

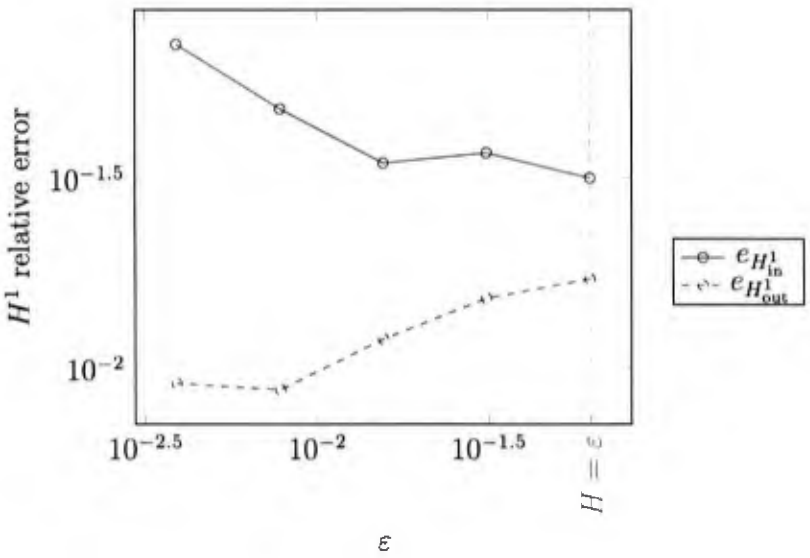

Figure 21: [Neumann Problem (18)] Sensitivity to the small scale ε: Adv-MsFEM with advective bubble functions ($\mathcal{O} = \mathcal{O}_1$).

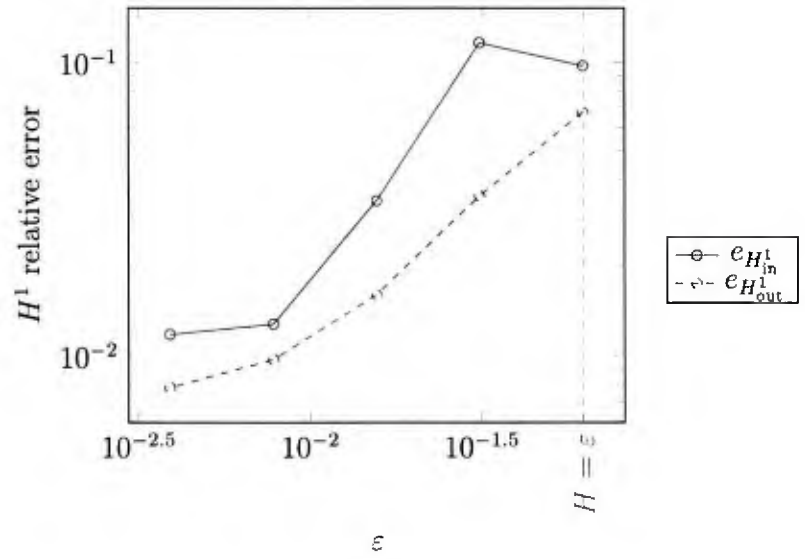

Figure 22: [Neumann Problem (18)] Sensitivity to the small scale ε: Adv-MsFEM with advective bubble functions ($\mathcal{O} = \mathcal{O}_2$).

of Stab-MsFEM (it may even degrade it). The results for $\mathcal{O} = \mathcal{O}_2$ are similar (results not shown).

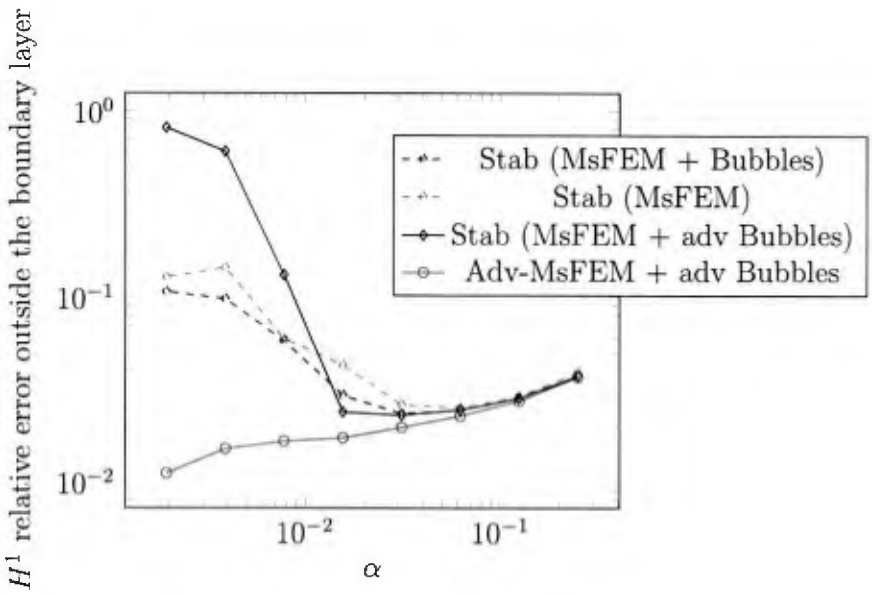

Figure 23: [Neumann Problem (18)] Adding bubbles to Stab-MsFEM: error outside the boundary layer ($\mathcal{O} = \mathcal{O}_1$).

4.3.2 A non-periodic case

A major motivation for using MsFEM approaches is to address non-periodic cases, for which homogenization theory does not provide any explicit approximation strategy. In this section, we assess the performance of our approaches on the non-periodic geometry $\Omega^\varepsilon_{\rm np}$ shown on Figure 24.

With the aim to investigate the robustness of our approaches with respect to the geometry of the perforations, we compare the results obtained in this non-periodic case with those obtained for a periodically perforated domain $\Omega^\varepsilon_{\rm p}$ defined by (36) with $\varepsilon = 0.03125$, $Y = (0,1)^2$ and $\mathcal{O} = r\mathcal{O}_1$ where $r > 0$ is such that $|\Omega^\varepsilon_{\rm p}| = |\Omega^\varepsilon_{\rm np}|$: the size of the small scale and the amount of perforations is thus identical for the two problems.

We study the influence of the Péclet number. We recall that we fix $\varepsilon = 0.03125$, $H = 1/16$ and we vary $\alpha = 2^k$, for integers $k = -9$ to -2. Figure 25 displays the relative H^1 broken error outside the boundary layer of our most accurate approaches, namely the Adv-MsFEM with advective bubble functions and the Stab-MsFEM. We observe that the Stab-MsFEM is insensitive to the non-periodicity of the geometry. The Adv-MsFEM with advective bubble functions is more sensitive to the non-periodicity of the geometry but still outperforms the Stab-MsFEM in both cases.

5 Conclusion and perspectives

The funding period 2015–2018 has enabled us to make significant progress both

(i) on the theoretical front, by better understanding the mathematical properties of linear

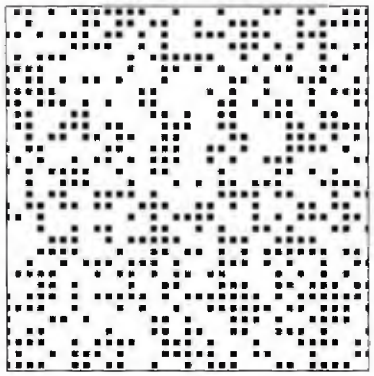

Figure 24: Non-periodic geometry. Let M_ε be the set of perforations obtained by periodically perforating the domain $\Omega = (0,1)^2$ by the motif $\mathcal{O}_2$ (we again denote $Y = (0,1)^2$ the periodic cell and set $\varepsilon = 0.03125$). Each of these perforations is next removed with a probability $1/2$, independently of all the other ones.

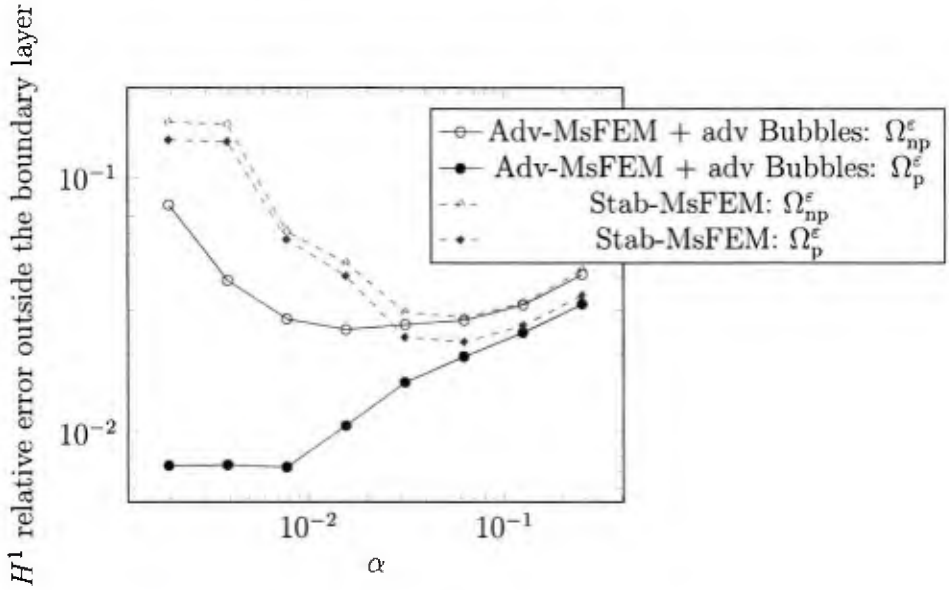

Figure 25: [Neumann Problem (18)] Sensitivity of the approaches to the non-periodicity of the geometry.

elliptic homogenization problems for periodic coefficients perturbed by globally integrable defects,

(ii) and on the numerical front, by deriving *a posteriori* estimators for MsFEM approaches, and discussing the adaptation of these approaches to advection dominated problems in the presence of perforations.

As always in a scientific endeavor, an improved knowledge of the problems considered raises even more interesting questions than before.

A natural follow-up theoretical study is to

(a) consider perturbations to periodicity that are more severe than perturbations vanishing at infinity (mathematically, in the L^p sense), such as perturbations that are "rare" but non necessarily vanishing at infinity (think of a sequence of bumps, all of size one – and therefore not globally integrable – but supported on regions of the space that are scarcer as one goes infinitely far away from the origin) or perturbations that in no way decay at infinity, but permanently perturb periodicity even infinitely far away (think of quasi random sequences).

(b) revisit the issue of perturbations to periodicity, even in the "simple" L^p sense (not to mention the compactly supported perturbations that may even lead to substantial difficulties), but for equations significantly more complicated than linear elliptic equations in divergence form, and equally important and practically relevant as the latter equations: quasilinear equations (e.g. the p-laplacian), fully nonlinear equations (Hamilton-Jacobi type equations), ...New mathematical questions, some of them challenging, will inevitably arise.

A long-term goal for this line of theoretical research would be to demonstrate that homogenization properties, even quantitative and explicit (meaning that formulae are available – and compute-able – for the homogenized tensors and the two-scale approximations, along with suitable rates of convergence) have nothing to do with rigid geometric properties such as periodicity – or likewise ergodic stationarity –, but only depend on much milder properties such as those related to the existence of averages on large volumes.

Similarly, our research on MsFEM type approaches paved the way to several possible tracks for continuation, in particular:

(c) the most part of the rigorous numerical analysis of multi-scale approaches (including MsFEM) is performed for self-adjoint problems, with only a few exceptions where non self-adjoint problems (such as advection-diffusion problems) are considered. In that latter case, the variants of the multi-scale approaches studied are very specific. It is definitely interesting (both theoretically and also with a definite practical purpose) to discriminate, both at an abstract level and also for more specific examples of approaches, where self-adjointness is essential and where it is unnecessary.

(d) thin structures such as plates or shells are often encountered in practice. In the homogeneous case, it is well known that theoretical difficulties (such as loss of ellipticity) and numerical difficulties (such as locking) may arise when simulating those. For heterogeneous structures, multi-scale approaches are needed. It is an interesting question to revisit the issues in a multiscale context, in order to design numerical approaches able to simultaneously cope with two small parameters, the thickness of the structure and the small characteristic size of the heterogeneities.

It is our desire to continue along some of the above proposed research directions in the context of a possible renewed ONR funding period.

References

References authored by the investigators in the context of the contract

[1] X. Blanc, M. Josien and C. Le Bris, *Approximation locale précisée dans des problèmes multi-échelles avec défauts localisés (Local precised approximation for multiscale problems with local defects)*, to appear in Note aux Comptes Rendus de l'Académie des Sciences, https://hal.archives-ouvertes.fr/hal-01893991.

[2] X. Blanc, M. Josien and C. Le Bris, *Precised approximations in elliptic homogenization beyond the periodic setting*, submitted, https://hal.archives-ouvertes.fr/hal-01958207.

[3] X. Blanc, C. Le Bris and P.-L. Lions, *On correctors for linear elliptic homogenization in the presence of local defects*, to appear in Communications in P.D.E., https://arxiv.org/abs/1801.10335.

[4] X. Blanc, C. Le Bris and P.-L. Lions, *On correctors for linear elliptic homogenization in the presence of local defects: the case of advection-diffusion*, to appear in Journal de Mathématiques Pures et Appliquées, https://arxiv.org/abs/1801.10330.

[5] L. Chamoin and F. Legoll, *A posteriori error estimation and adaptive strategy for the control of MsFEM computations*, Computer Methods in Applied Mechanics and Engineering, 336:1–38, 2018.

[6] L. Chamoin and F. Legoll, *Goal-oriented error estimation and adaptivity in MsFEM computations*, manuscript in preparation.

[7] C. Le Bris, F. Legoll and S. Lemaire, *On the best constant matrix approximating an oscillatory matrix-valued coefficient in divergence-form operators*, to appear in Control Optim. Calc. Var., https://arxiv.org/abs/1612.05807.

[8] C. Le Bris, F. Legoll and F. Madiot, *Multiscale Finite Element methods for advection-dominated problems in perforated domains*, submitted to SIAM Multiscale Modeling & Simulation, https://arxiv.org/abs/1710.09331.

References authored by the investigators and not related to the current ONR contract

[9] X. Blanc, C. Le Bris and P.-L. Lions, *A possible homogenization approach for the numerical simulation of periodic microstructures with defects*, Milan Journal of Mathematics, 80:351–367, 2012.

[10] X. Blanc, C. Le Bris and P.-L. Lions, *Local profiles and elliptic problems at different scales with defects*, Note aux Comptes Rendus de l'Académie des Sciences, Série I, 353:203–208, 2015.

[11] X. Blanc, C. Le Bris and P.-L. Lions, *Local profiles for elliptic problems at different scales: defects in, and interfaces between periodic structures*, Communications in P.D.E., 40(12):2173–2236, 2015.

[12] C. Le Bris, F. Legoll and A. Lozinski, *MsFEM à la Crouzeix-Raviart for highly oscillatory elliptic problems*, Chinese Annals of Mathematics, Series B, 34(1):113–138, 2013.

[13] C. Le Bris, F. Legoll and A. Lozinski, *An MsFEM type approach for perforated domains*, SIAM Multiscale Modeling & Simulation, 12(3):1046–1077, 2014.

[14] C. Le Bris, F. Legoll and F. Madiot, *A numerical comparison of some Multiscale Finite Element approaches for advection-dominated problems in heterogeneous media*, Mathematical Model. Numer. Anal., 51(3):851–888, 2017.

[15] C. Le Bris, F. Legoll and W. Minvielle, *Multiscale materials science: a mathematical approach to the role of defects and uncertainty*, ONR report 2015.

General references by other authors

[16] G. Allaire and R. Brizzi, *A multiscale finite element method for numerical homogenization*, SIAM Multiscale Modeling & Simulation, 4(3):790–812, 2006.

[17] M. Avellaneda and F.H. Lin, *Compactness methods in the theory of homogenization*, Commun. Pure Appl. Math., 40(6):803–847, 1987.

[18] M. Avellaneda and F.H. Lin, *Compactness methods in the theory of homogenization. II: Equations in non-divergence form*, Commun. Pure Appl. Math., 42(2):139–172, 1989.

[19] M. Avellaneda and F.H. Lin, *L^p bounds on singular integrals in homogenization*, Commun. Pure Appl. Math., 44(8-9):897–910, 1991.

[20] A. Bensoussan, J.-L. Lions and G. Papanicolaou, **Asymptotic analysis for periodic structures**, Studies in Mathematics and its Applications, vol 5. North-Holland Publishing Co., Amsterdam-New York, 1978.

[21] Y. Efendiev and T. Hou, **Multiscale Finite Element Methods: Theory and Applications**, Springer, New York 2009.

[22] Y. Efendiev, T. Hou and X.H. Wu, *Convergence of a nonconforming multiscale finite element method*, SIAM Journal of Numerical Analysis, 37(3):888–910, 2000.

[23] P. Henning, M. Ohlberger and B. Schweizer, *An adaptive multiscale finite element method*, SIAM Multiscale Modeling & Simulation, 12(3):1078–1107, 2014.

[24] U. Hornung, **Homogenization and porous media**, Springer, 1997.

[25] P. Ladevèze and J.-P. Pelle, **Mastering Calculations in Linear and Nonlinear Mechanics**, Springer, 2004.

[26] A. Quarteroni and A. Valli, **Numerical approximation of partial differential equations**, Springer Series in Computational Mathematics, vol. 23, Springer, 1994.